Anxiety-related frontocortical activity is associated with dampened stressor reactivity in the real world

Juyoen Hur[1]*
Manuel Kuhn[2]*
Shannon E. Grogans[3]*
Allegra S. Anderson[7]
Samiha Islam[8]
Hyung Cho Kim[3,5]
Rachael M. Tillman[3]
Andrew S. Fox[9]
Jason F. Smith[3]†
Kathryn A. DeYoung[3,4]†
Alexander J. Shackman[3,5,6]†

[1]Department of Psychology, Yonsei University, Seoul 03722, Republic of Korea. [2]Center for Depression, Anxiety and Stress Research, McLean Hospital, Harvard Medical School, Belmont, MA 02478 USA. Departments of [3]Psychology, and [4]Family Science; [5]Neuroscience and Cognitive Science Program; and [6]Maryland Neuroimaging Center, University of Maryland, College Park, MD 20742 USA. [7]Department of Psychological Sciences, Vanderbilt University, Nashville, TN 37240 USA. [8]Department of Psychology, University of Pennsylvania, Philadelphia, PA USA. [9]Department of Psychology and California National Primate Research Center, University of California, Davis, CA 95616 USA

* contributed equally * | † contributed equally

Figures: 5

Additional Elements: Supplementary results

Keywords: emotion, extended amygdala, fear and anxiety, functional MRI (fMRI), individual differences, negative affect

Address Correspondence to:
Juyoen Hur (jhur1@yonsei.ac.kr) or Alexander J. Shackman (shackman@umd.edu)

ACKNOWLEDGEMENTS

This work was supported by the NIH (MH107444, MH121409, MH121735). Authors declare no conflicts of interest.

RESOURCE SHARING

Raw data (https://nda.nih.gov) and processed EMA data (https://github.com/dr-consulting/shackman-umd-pax-ema-pub) are available. Key neuroimaging maps will be uploaded to NeuroVault.org.

ABSTRACT

Negative affect is a fundamental dimension of human emotion. When extreme, it contributes to a variety of adverse outcomes—from physical and mental illness to divorce and premature death. Mechanistic work in animals and neuroimaging research in humans has begun to reveal the broad contours of the neural circuits governing negative affect, but the relevance of these discoveries to everyday distress remains incompletely understood. Here we used a combination of approaches—including neuroimaging assays of threat anticipation and perception, >10,000 momentary assessments of emotional experience, and large-scale automated analyses of regional connectivity and co-activation—to demonstrate that individuals showing greater activation in a cingulo-opercular circuit during an anxiety-eliciting laboratory paradigm experience lower levels of stressor-dependent distress in their daily lives. Subcortical activation was not significantly related to momentary negative affect. These observations provide a framework for understanding the neurobiology of negative affect in the laboratory and in the real world.

STATEMENT OF RELEVANCE

Anxiety, sadness, and other negative emotions are hallmarks of the human condition. When extreme, they contribute to a variety of adverse outcomes—from physical and mental illness to divorce and premature death—pointing to the need to develop a better understanding of the underlying brain circuitry. Recent work has begun to reveal the neural systems governing negative affect, but the relevance of these tantalizing laboratory discoveries to the real world has remained unclear. Here we used a combination of brain imaging and smartphone-based survey techniques to demonstrate that individuals evincing greater activation in a cingulo-opercular circuit during an anxiety-promoting laboratory task experienced reduced distress in the moments following exposure to daily stressors. These observations provide new insights into the brain systems most relevant to negative emotion in everyday life, underscoring the importance of more recently evolved cortical association areas.

INTRODUCTION

Negative affect is a fundamental dimension of mammalian emotion. It encompasses transient states—like fear, anxiety, sadness, and worry—and more persistent, trait-like tendencies to experience and express such states (Shackman et al., 2016). When extreme or pervasive, negative affect contributes to a panoply of adverse outcomes—from physical and mental illness to divorce and premature death—underscoring the need to develop a better understanding of the underlying neurobiology (Hur, Stockbridge, Fox, & Shackman, 2019).

Mechanistic work in animals and neuroimaging research in humans has begun to reveal the broad contours of the neural systems governing negative affect (Chang, Gianaros, Manuck, Krishnan, & Wager, 2015; Fox & Shackman, 2019; Horikawa, Cowen, Keltner, & Kamitani, 2020; Kenwood & Kalin, 2021; Taschereau-Dumouchel, Kawato, & Lau, 2019). This work underscores the importance of *subcortical* regions, like the amygdala, bed nucleus of the stria terminalis (BST), and periaqueductal gray (PAG). But it also highlights *frontocortical* regions that are particularly well developed in humans, including the midcingulate cortex (MCC), anterior insula (AI), frontal operculum (FrO), and dorsolateral prefrontal cortex (dlPFC) (Hur et al., 2020b; Shackman & Fox, 2021; Shackman et al., 2011). At present, the relevance of these tantalizing laboratory discoveries to subjective emotional experience in the real world remains incompletely understood. Given the limitations of ambulatory measures of brain activity—there is no 'fMRI helmet' as yet—overcoming this barrier requires integrating measures of emotion-relevant brain function acquired in the laboratory with assessments of negative affect collected in the field.

Here we used fMRI to quantify individual differences in neural reactivity to a well-established anxiety-provocation ('threat-anticipation') paradigm in 220 young adults, a sample ~8 times larger than typical

fMRI studies (Poldrack et al., 2017) (**Figure 1**). A multiband sequence and best-practice data processing techniques enhanced our ability to resolve small subcortical regions, like the amygdala and BST. Next, we used smartphone experience sampling or 'ecological momentary assessment' (EMA)—to intensively sample fluctuations in self-reported negative affect and stressor exposure across different real-world contexts. To ensure a broad spectrum of emotional reactivity, subjects were selectively recruited from a pool of 6,594 young adults screened for trait-like individual differences in negative emotionality (Hur et al., 2020a). We focused on 'emerging adulthood' because it is a time of profound, often stressful transitions (Shackman et al., 2018). In fact, more than half of undergraduate students report moderate-to-severe levels of anxiety and depression, with many experiencing frank emotional disorders during this turbulent developmental chapter (GBD 2019 Diseases and Injuries Collaborators, 2020; National Academies of Sciences, Engineering, & Medicine, 2021; Substance Abuse and Mental Health Services Administration, 2019).

As shown schematically in **Figure 1**, hierarchical linear models (HLMs) were used to fuse the fMRI and EMA data-streams, allowing us to selectively probe relations between anxiety-related brain function and *tonic* (stressor-independent) and *reactive* (stressor-dependent) variation in real-world negative affect (Gross, Sutton, & Ketelaar, 1998; Shackman et al., 2016). To clarify specificity, parallel analyses were performed for positive affect and positive events. This approach also allowed us to quantify the added explanatory value ('incremental validity') of neuroimaging metrics relative to a conventional paper-and-pencil measure of trait negative emotionality (Shackman & Fox, 2018).

Aside from addressing the real-world significance of anxiety-related neural circuitry, this approach afforded an opportunity to clarify the contributions of frontocortical regions to negative affect. Although the MCC, AI/FrO, and dlPFC are consistently recruited by a variety of distress-eliciting experimental

challenges, their precise role has remained enigmatic (Hur et al., 2020b). In part, this reflects the fact that a broadly similar network is recruited by emotion-regulation paradigms (Langner, Leiberg, Hoffstaedter, & Eickhoff, 2018; Morawetz et al., 2020), raising the possibility that frontocortical activation actually reflects spontaneous efforts to dampen, rather than promote, distress. Fusing the fMRI and EMA data streams enabled us to test whether frontocortical activity is associated with increased or decreased levels of negative affect in the midst of daily life.

To provide a more direct link with prior and on-going research, we conducted parallel analyses using fMRI data acquired from a subset of subjects who had also completed an emotional-faces fMRI paradigm. Variants of this paradigm are widely used as probes of amygdala function—often in the guise of quantifying variation in 'Negative Valence Systems'—and have been incorporated into many biobank studies, including ABCD (Casey et al., 2018), Duke Neurogenetics (Elliott et al., 2019), the Human Connectome Project (HCP) and follow-ons (Barch et al., 2013; Seok et al., 2020; Siless et al., 2020; Somerville et al., 2018; Tozzi et al., 2020), IMAGEN (Albaugh et al., 2019), the Philadelphia Neurodevelopmental Cohort (Satterthwaite et al., 2016), and UK Biobank (Miller et al., 2016). Although photographs of models posing 'threat-related' (i.e., fearful and angry) facial displays strongly activate the amygdala (Miller et al., 2016), they do not elicit distress in typical adult populations and, as such, are better conceptualized as indices of emotion perception, rather than emotional experience or expression (Hur et al., 2019). Here, we determined whether differences in face-elicited amygdala activation are associated with EMA measures of negative affect (**Figure 1**).

Discovering the neural systems most relevant to the moment-by-moment experience of negative affect in daily life is important. Emotional illnesses are defined, diagnosed, and treated on the basis of real-world feelings, and for some theorists they are *the* defining feature of emotion (Fox, Lapate, Shackman, &

Davidson, 2018; LeDoux & Pine, 2016; Mobbs et al., 2019). This approach has the potential to provide insights that cannot be achieved using either animal models or isolated measures of human brain function and represents a step to establishing the everyday relevance of the brain circuits highlighted in laboratory studies of emotion generation and perception.

METHOD

Overview

As part of an on-going prospective-longitudinal study focused on the emergence of mood and anxiety disorders, we used measures of trait negative emotionality (often termed neuroticism or dispositional negativity; Hur et al., 2020a; Shackman et al., 2018) to screen 6,594 young adults (57.1% female; 59.0% White, 19.0% Asian, 9.9% African American, 6.3% Hispanic, 5.8% Multiracial/Other; M=19.2 years, SD=1.1 years). Screening data were stratified into quartiles (top quartile, middle quartiles, bottom quartile) separately for men and women. Individuals who met preliminary inclusion criteria were independently and randomly recruited from each of the resulting six strata. Given the focus of the larger study, approximately half the subjects were recruited from the top quartile, with the remainder split between the middle and bottom quartiles (i.e., 50% high, 25% medium, and 25% low), enabling us to sample a wide range of risk for the development of internalizing disorders. Simulation work suggests that this enrichment' approach does not bias statistical tests to a degree that would compromise their validity (Hauner, Zinbarg, & Revelle, 2014). All subjects were first-year university students in good physical health with normal or corrected-to-normal color vision and access to a smartphone. All reported the absence of a lifetime neurological or pervasive developmental disorder, medical conditions that would contraindicate MRI, or prior experience with noxious electrical stimulation. All subjects were free from a lifetime history of psychotic and bipolar disorders; a current diagnosis of a mood, anxiety, or trauma disorder (past 2 months); severe substance abuse; active suicidality; and on-going psychiatric treatment

as determined by an experienced masters-level diagnostician using the Structured Clinical Interview for DSM-5 (First, Williams, Karg, & Spitzer, 2015). To maximize the range of psychiatric risk, subjects with a lifetime history of anxiety and mood disorders were not excluded. At the baseline laboratory session, subjects provided informed written consent, were familiarized with the EMA protocol (see below), and re-completed the trait negative emotionality assessment. Beginning the next day, subjects completed up to 8 EMA surveys per day for 7 days (see below for compliance). Subjects completed a neuroimaging assessment within five weeks of the EMA protocol (*Median* = 13 days, *Max* = 39 days). All procedures were approved by the University of Maryland Institutional Review Board. The sample overlaps that featured in work by our group focused on social anxiety and momentary mood (Hur et al., 2020a) and the basic neurobiology of threat processing (Hur et al., 2020b).

Subjects

A total of 234 subjects completed the MRI assessment.

Anxiety provocation. Fourteen subjects were excluded from fMRI analyses of the anxiety-provocation task due to incidental neurological findings (n=4), scanner problems (n=2), insufficient usable fMRI data (n=2; see below), or excessive global motion artifact (n=6; see below). Twelve subjects did not successfully complete the EMA assessment (see below), and were excluded from fMRI-EMA analyses. This yielded a final sample of 208 subjects (50.0% female; 63.0% White, 17.3% Asian, 8.2% African American, 3.8% Hispanic, 7.7% Multiracial/Other; M = 18.8 years, SD = 0.4).

Threat-Related Faces. Twenty-one subjects were excluded from fMRI analyses of the threat-related faces task due to incidental neurological findings (n=4), scanner problems (n=2), gross artifacts (n=1), insufficient usable fMRI data (n=1; see below), excessive global motion artifact (n=7; see below), or

inadequate performance accuracy (n=6; see below). Eleven subjects did not successfully complete the EMA assessment (see below), and were excluded from fMRI-EMA analyses. This yielded a final sample of 202 subjects (50.0% female; 63.4% White, 16.8% Asian, 8.4% African American, 4.0% Hispanic, 7.4% Multiracial/Other; M = 18.8 years, SD = 0.4).

Power Analysis

Sample size was determined *a priori* as part of the application for the award that supported data collection (R01-MH107444). The target sample size ($N \approx 240$) was chosen to afford acceptable power and precision given available resources (Schönbrodt & Perugini, 2013). At the time of study design, G-power 3.1.9.2 (http://www.gpower.hhu.de) indicated >99% power to detect a benchmark medium-sized effect (r = .30) with up to 20% planned attrition (N = 192 usable datasets) using α = .05 (two-tailed).

Trait Negative Emotionality

As in prior work (Hur et al., 2020a; Shackman et al., 2018), we used measures of neuroticism (Big Five Inventory-Neuroticism, α = 0.86-0.89; John, Naumann, & Soto, 2008) and trait anxiety (International Personality Item Pool-Trait Anxiety, α = 0.89; Goldberg, 1999; Goldberg et al., 2006) to quantify individual differences in negative emotionality. Subjects used a 1 (*disagree strongly*) to 5 (*agree strongly*) scale to rate themselves on a total of 18 items (e.g., *depressed or blue, tense, worry, nervous, get distressed easily, fear for the worst, afraid of many things*). To minimize the influence of occasion-specific fluctuations in responding (Mõttus et al., 2020), analyses of incremental validity employed a measure averaged across assessments (median interval = 80.0 days, SD = 56.6). The resulting composite captured a sizable range of the trait negative affect spectrum (z = -2.11 to 1.49) and showed acceptable reliability (α = 0.93, r_{Retest} = .75).

General Neuroimaging Procedures

Prior to scanning, subjects practiced abbreviated versions of the tasks until staff confirmed their understanding. A detailed description of the peripheral apparatus is available (Hur et al., 2020b). During imaging, foam inserts were used to mitigate potential motion artifacts. Subjects were continuously monitored using an MRI-compatible eye-tracker (Eyelink 1000; SR Research, Ottawa, Ontario, Canada). Head motion was monitored using the AFNI real-time plugin (Cox, Jesmanowicz, & Hyde, 1995). Following the last scan, subjects were removed from the scanner, debriefed, compensated, and discharged.

Anxiety-Provocation Paradigm

Paradigm Structure and Procedures. A detailed description of the anxiety-provocation (threat-anticipation) paradigm and associated procedures and stimuli is available (Hur et al., 2020b). Subjects were completely informed about the task design and contingencies prior to scanning. The task was administered in 3 scans, with a short break between scans (12 trials/condition/scan). On Threat trials, subjects saw a stream of integers (M=18.75 s; 8.75-30.00 s). To ensure robust anticipatory anxiety, this epoch always culminated with the delivery of a noxious electric shock, unpleasant photograph (e.g. mutilated body), and thematically related audio clip (e.g. scream, gunshot). Mean duration was chosen to enhance detection of task-related differences in the blood oxygen level-dependent (BOLD) signal (Henson, 2007a). Safety trials were similar, but terminated with the delivery of benign reinforcers (i.e., just-perceptible electrical stimulation and neutral audiovisual stimuli; see below). Valence was continuously signaled during the anticipation epoch by the background color of the display. White-noise visual masks (3.2 s) were presented between trials to minimize persistence of the visual reinforcers in

iconic memory. Subjects were periodically prompted to rate the intensity of negative affect ('fear/anxiety') experienced a few seconds earlier, during the *anticipation* period of the prior trial, using a 1 (*minimal*) to 4 (*maximal*) scale. Each condition was rated twice per scan, for a total of 6 ratings per condition. The intensity of electrical stimulation was individually titrated prior to data collection (for details, see Hur et al., 2020b).

Skin Conductance Data Acquisition and Processing Pipeline. To confirm the validity of the anxiety-provocation paradigm, skin conductance was continuously assessed during each scan of the anxiety-provocation task using a Biopac system (MP-150; Biopac Systems, Inc., Goleta, CA). Skin conductance (250 Hz; 0.05 Hz high-pass) was measured using MRI-compatible disposable electrodes (EL507) attached to the second and third fingers of the non-dominant hand. Skin conductance data were processed using PsPM (version 4.0.2) and in-house MATLAB code (Bach et al., 2018; Bach & Friston, 2013). Data from each scan were band-pass filtered (0.01-0.25 Hz), resampled to match the TR used for fMRI data acquisition (1.25 s), and *z*-transformed.

Threat-Related Faces Paradigm

The faces paradigm took the form of a randomized block design and was administered in 2 scans, with a short break between each scan. During each scan, subjects viewed photographs of angry faces, fearful faces, happy faces, or places (7 blocks/condition/scan). To maximize signal strength and homogeneity, and minimize potential habituation (Henson, 2007b; Maus, van Breukelen, Goebel, & Berger, 2010; Plichta et al., 2014), each block consisted of 10 photographs (1.4 s/image) separated by the brief presentation of a fixation cross (0.6 s). To maximize task engagement, on each trial, subjects judged whether the identity of the current photograph matched that on the prior trial (i.e., a '1-back' continuous

performance task). Matches occurred 37% of the time. Face stimuli were adapted from prior work (Gamer, Schmitz, Tittgemeyer, & Schilbach, 2013; Scheller, Büchel, & Gamer, 2012) and included standardized images of male and female adults displaying unambiguous emotional expressions. To maximize the number of models and further mitigate potential habituation, face stimuli were derived from multiple databases: Ekman and Friesen's Pictures of Facial Affect (Ekman & Friesen, 1976), the FACES database (Ebner, Riediger, & Lindenberger, 2010), the Karolinska Directed Emotional Faces database (http://www.emotionlab.se/resources/kdef), and the NimStim Face Stimulus Set (https://www.macbrain.org/resources.htm). Color images were converted to grayscale, brightness normalized, and masked to occlude non-facial features. Place stimuli were also adapted from prior work (Choi, Padmala, & Pessoa, 2012, 2015), and included grayscale photographs of outdoor scenes focused on single-family residential buildings ('houses') or urban commercial buildings ('skyscrapers'). Subjects showing inadequate performance (i.e., accuracy <2 *SD* for both scans) were excluded from analyses.

MRI Data Acquisition

MRI data were acquired using a Siemens Magnetom TIM Trio 3 Tesla scanner (32-channel head-coil). Sagittal T1-weighted anatomical images were acquired using a magnetization prepared rapid acquisition gradient echo (MPRAGE) sequence (TR=2,400 ms; TE=2.01 ms; inversion time=1060 ms; flip angle=8°; sagittal slice thickness=0.8 mm; in-plane=0.8 × 0.8 mm; matrix=300 × 320; field-of-view=240 × 256). A T2-weighted image was collected co-planar to the T1-weighted image (TR=3,200 ms; TE=564 ms; flip angle=120°). To enhance resolution, for both tasks, a multi-band sequence was used to collect oblique-axial echo planar imaging (EPI) volumes (multiband acceleration=6; TR=1,250 ms; TE=39.4 ms; flip angle=36.4°; slice thickness=2.2 mm, number of slices=60; in-plane resolution=2.1875 × 2.1875 mm; matrix=96 × 96). Images were collected in the oblique axial plane (approximately −20° relative to the AC-

PC plane) to minimize potential susceptibility artifacts (anxiety provocation: 478 volumes/scan; faces: 454 volumes/scan). The first 7 volumes were automatically discarded by the scanner. To enable field map correction, two oblique-axial spin echo (SE) images were collected in opposing phase-encoding directions (rostral-to-caudal and caudal-to-rostral) at the same location and resolution as the functional volumes (i.e., co-planar; TR=7,220 ms, TE=73 ms).

MRI Data Processing Pipeline

Methods were optimized to minimize spatial normalization error and potential sources of noise. Structural and functional MRI data were visually inspected before and after processing for quality assurance.

Anatomical Data. Methods were similar to those employed in recent reports by our group (e.g., Hur et al., 2020b). T1-weighted images were inhomogeneity corrected using N4 (Tustison et al., 2010) and filtered using the denoise function in ANTS (Avants et al., 2011). The brain was then extracted using a variant of BEaST (Eskildsen et al., 2012) with brain-extracted and normalized reference brains from the IXI database (https://brain-development.org/ixi-dataset). Brain-extracted T1 images were normalized to a version of the brain-extracted 1-mm T1-weighted MNI152 (version 6) template (Grabner et al., 2006) customized to remove extracerebral tissue. This was motivated by evidence that brain-extracted T1 images and templates enhance the quality of spatial normalization (Acosta-Cabronero, Williams, Pereira, Pengas, & Nestor, 2008; Fein et al., 2006; Fischmeister et al., 2013). Normalization was performed using the diffeomorphic approach implemented in SyN (version 1.9.x.2017-09.11; Avants et al., 2011; Klein et al., 2009). T2-weighted images were rigidly co-registered with the corresponding T1 prior to normalization and the brain extraction mask from the T1 was applied. Tissue priors (Lorio et al., 2016)

were unwarped to the native space of each T1 using the inverse of the diffeomorphic transformation. Brain-extracted T1 and T2 images were simultaneously segmented using native-space priors generated using FAST (FSL version 5.0.9; Zhang, Brady, & Smith, 2001) for use in T1-EPI co-registration (see below).

Field Map Data. SE images were used to create a field map in topup (Andersson, Skare, & Ashburner, 2003; Graham, Drobnjak, & Zhang, 2017; Smith et al., 2004). Field maps were converted to radians, median filtered, and smoothed (2-mm). The average of the distortion-corrected SE images was inhomogeneity-corrected using N4 and brain-masked using 3dSkullStrip in AFNI (version 17.2.10; Cox, 1996). The resulting mask was minimally eroded to further exclude extracerebral voxels.

Functional Data. EPI files were de-spiked (3dDespike) and slice-time corrected (to the center of the TR) using 3dTshift, inhomogeneity corrected using N4, and motion corrected to the first volume using a 12-parameter affine transformation implemented in ANTs. Recent work indicates that de-spiking is more effective than 'scrubbing' for attenuating motion-related artifacts (Jo et al., 2013; Power, Schlaggar, & Petersen, 2015; Siegel et al., 2014). Transformations were saved in ITK-compatible format for subsequent use. The first volume was extracted for EPI-T1 co-registration. The reference EPI volume was simultaneously co-registered with the corresponding T1-weighted image in native space and corrected for geometric distortions using boundary-based registration (Greve & Fischl, 2009). This step incorporated the previously created field map, undistorted SE, T1, white matter (WM) image, and masks. The spatial transformations necessary to transform each EPI volume from native space to the reference EPI, from the reference EPI to the T1, and from the T1 to the template were concatenated and applied to the processed (de-spiked and slice-time corrected) EPI data in a single step to minimize incidental spatial

blurring. Normalized EPI data were resampled to 2-mm isotopic voxels using fifth-order b-splines and smoothed (6-mm FWHM) using 3DblurInMask.

EMA Protocol, Measures, and Data Reduction

Protocol. As in other work by our group (Doorley et al., *in press*; Doorley, Volgenau, Kelso, Kashdan, & Shackman, 2020; Hur et al., 2020a; Shackman et al., 2018), SurveySignal was used to automatically deliver 8 text messages/day to each subject's smartphone (Hofmann & Patel, 2015). Messages were delivered between 8:30 AM and 11 PM, with 1.5-3 hours between successive messages (M = 120 minutes, SD = .43). During weekdays, messages were delivered during the 'passing periods' between scheduled university courses to reduce burden and maximize compliance. Messages were delivered according to a fixed schedule that varied across days (e.g., the third message was delivered at 12:52 PM on Mondays and 12:16 PM on Tuesdays). Messages contained a link to a secure on-line survey. Subjects were instructed to respond within 30 minutes (*Median* = 2 min, SD = 7 min) and to refrain from responding at unsafe or inconvenient moments (e.g., while driving). During the baseline laboratory session, several procedures were used to promote compliance (Palmier-Claus et al., 2011) including: (a) delivering a test message to the subject's phone and confirming that they were able to successfully complete the on-line survey, (b) providing subjects with a 24/7 technical support number, and (c) providing monetary bonuses for increased compliance.

EMA Survey and Data Reduction. Current negative affect (*afraid, nervous, worried, hopeless, sad*) and positive affect (*calm, cheerful, content, enthusiastic, joy, relaxed*) at the time of the survey prompt was rated using a 0 (*not at all*) to 4 (*extremely*) scale. Stressor exposure was assessed using an additional binary item (*Did you experience one or more negative events in the past hour?)*. A parallel item was used to

assess recent exposure to positive events. Composite measures of negative and positive affect were computed by averaging relevant items (α = .80-.88). Conclusions remained identical using square-root transformed negative affect (not reported). To better understand the nature of significant brain-EMA relations, follow-up tests employed composite anxiety (*afraid, nervous, worried*) and depression (*hopeless, sad*) facet scales (αs = .66-.79). EMA compliance was acceptable (*M* = 87.9%, *SD* = 6.1%, Minimum = 71.4%, Total assessments = 10,239), and key results remained significant after controlling for variation in compliance (not reported).

Skin Conductance Modeling

Using standard MATLAB functions, SCR data were modeled using an approach similar to that used for the fMRI data. A general linear model (GLM) was used to estimate skin conductance levels during the anticipatory epoch of each condition of the anxiety-provocation paradigm for each subject (Bach, 2014; Bach, Flandin, Friston, & Dolan, 2009; Bach, Friston, & Dolan, 2013). Predictors from the first-level fMRI model (see below) were convolved with a canonical skin conductance response function (Bach, Flandin, Friston, & Dolan, 2010; Gerster, Namer, Elam, & Bach, 2018), bandpass filtered to match the data, and *z*-transformed.

fMRI Modeling and Data Reduction

Data Exclusions. To assess residual global motion artifact, we computed average volume-to-volume displacement for each scan using the motion-corrected data. Scans with excess artifact (>2 *SD*) were discarded. Subjects who lacked sufficient usable fMRI data (<2 scans per task) or showed inadequate performance on the emotional-faces task (see above; accuracy <2 *SD*) were excluded from analyses.

First-Level fMRI Models. Modeling was performed using SPM12 (version 6678) (https://www.fil.ion.ucl.ac.uk/spm) and custom MATLAB scripts. Temporal band-pass was set to the hemodynamic response function (HRF) and 128 s for low and high pass, respectively. Regressors were convolved with a canonical HRF and temporal derivative. Nuisance variates included framewise displacement, motion parameters, cerebrospinal fluid time-series, and instantaneous pulse and respiration. ICA-AROMA (Pruim et al., 2015) was used to extract other potential sources of noise (e.g., white matter signal) and these were also included as nuisance variates, consistent with recent recommendations (Bijsterbosch et al., 2020). Volumes with framewise displacement >0.5 mm were censored. ***Anxiety Provocation.*** A detailed description of the modeling procedure is available elsewhere (Hur et al., 2020b). In brief, the anxiety-provocation task was modeled using variable-duration rectangular regressors time-locked to the anticipation epochs of Threat or Safety trials, to the presentation of aversive or benign stimulation, and to rating trials. Volumes coincident with aversive stimulation were censored. ***Emotional Faces.*** The emotional faces task was modeled using fixed-duration rectangular regressors time-locked to the blocks of angry, fearful, or happy faces.

Brain Metrics. To enable fusion of the fMRI and EMA data-streams, regions of interest were functionally prescribed based on significant task effects in whole-brain voxel-wise analyses (FDR $q < 0.05$, whole-brain corrected; see below) within anatomical regions selected based on prior large-scale studies and meta-analyses (e.g., Chavanne & Robinson, 2021; Hur et al., 2018; Hur et al., 2020b), consistent with recent recommendations (Bijsterbosch et al., 2020). It merits comment that this is a conservative approach. This reflects the fact that task effects (Student's t) are estimated by dividing the average within-individual difference (e.g., Threat vs. Safety) by the variation across individuals. All else being equal, regions showing stronger task effects will tend to show less between-subject variance and, hence, weaker relations with external variables (e.g., EMA affect). For each region (e.g., MCC) and subject,

regression coefficients were extracted and averaged across voxels using cubical masks centered on the local maxima identified in voxelwise analyses (**Figure 2**). A smaller 'faces-only' ROI (7 voxels, 56 mm^3) was used for subcortical regions, whereas a larger 'faces, edges, and corners' ROI (27 voxels, 216 mm^3) was used for cortical regions, consistent with other EMA-fMRI research (e.g., Lopez, Hofmann, Wagner, Kelley, & Heatherton, 2014). As a validity check, one-sample *t*-tests were used to confirm the sign and magnitude of ROI-extracted values (not reported). ***Anxiety Provocation.*** For the anxiety-provocation paradigm, analyses focused on activation during the anticipation of aversive compared to benign stimulation. Regression coefficients for the resulting 'Threat-versus-Safety' contrast were extracted and averaged across voxels for the dorsal amygala, BST, PAG, MCC, AI, FrO, and dlPFC. With the exception of the PAG—a small midline structure—coefficients were separately extracted for the left and right hemisphere, yielding a total of 13 ROIs. To minimize the number of comparisons, a factor analysis was used to further reduce data dimensionality (principal components extraction; oblimin rotation). Consistent with recent methodological recommendations (Lim & Jahng, 2019), parallel analysis (PA)—which compares the eigenvalues of the sample correlation matrix to those obtained using random uncorrelated standardized normal variables—was used to determine the number of factors to retain. PA was implemented using the *nFactors* package (version 2.4.1.) for *R*. Visual inspection of the scree plot, the Kaiser criterion (eigenvalue > 1), and PA all indicated the presence of 2 factors, with frontocortical ROIs loading on the first and subcortical ROIs loading on the second (**Supplementary Table S3**). Similar results were yielded using varimax rotation (not reported). Based on this, we standardized (*z*-transformation) and averaged the ROI values to create composite measures of frontocortical (α = .89) and subcortical activity (α = .82) for each subject. This approach is widely used in the social and biological sciences (e.g., Doré, Weber, & Ochsner, 2017; Fox et al., 2015; Lopez et al., 2017; Moffitt et al., 2011) and reduced the neuroimaging dataset from tens of thousands of voxels to two regional composites. ***Threat-Related Faces.*** For the faces paradigm, analyses focused on dorsal amygdala activity elicited by threat-related (i.e., fearful or angry) faces compared to places, consistent with prior work (e.g.,

Swartz, Knodt, Radtke, & Hariri, 2015). Paralleling the anxiety-provocation paradigm, mean coefficients were separately extracted for the left and right amygdalae, standardized, and averaged for each subject (α = .82).

Hypothesis Testing Strategy

Unless noted otherwise, hypothesis testing was performed using SPSS (version 24.0.0.0) and restricted maximum likelihood estimates. To guard against error, a second analyst independently analyzed and confirmed key results.

In-Scanner Distress Ratings and Skin Conductance. To confirm the validity of the anxiety-provocation paradigm, repeated-measures GLMs were used to test differences between Threat and Safety anticipation. Unfortunately, the sparse nature of the in-scanner ratings protocol (i.e., two ratings per condition in each scan) precluded meaningful analyses of concurrent brain-behavior relations. Raincloud plots were generated using open-source code (Allen, Poggiali, Whitaker, Marshall, & Kievit, 2019; van Langen, 2020).

fMRI. Standard whole-brain voxelwise GLMs with random effects were computed using SPM12 and used to assess activation to the anxiety-provocation (threat-anticipation) and emotional-faces paradigms. Significance was assessed using FDR q<.05, whole-brain corrected. Some figures were created using MRIcron (http://people.cas.sc.edu/rorden/mricron) and MRIcroGL (https://www.nitrc.org/projects/mricrogl). Clusters and local maxima were labeled using a combination of the Allen Institute, Harvard–Oxford, and Mai atlases (Desikan et al., 2006; Frazier et al., 2005; Hawrylycz et al., 2012; Mai, Majtanik, & Paxinos, 2015; Makris et al., 2006) and a recently established consensus nomenclature (ten Donkelaar, Tzourio-Mazoyer, & Mai, 2018). Frontal operculum subdivisions

were labeled using the nomenclature of Amunts (Amunts et al., 2010). Amygdala subdivisions were labeled using the atlases and recently developed ROIs (Tillman et al., 2018; Tyszka & Pauli, 2016).

Brain-EMA Fusion. As shown schematically in **Figure 1**, a series of HLMs—often termed 'multilevel' or 'linear mixed' models—was used to test relations between individual differences in task-related activation and momentary levels of *tonic* (stressor-independent) and *reactive* (stressor-dependent) negative affect, separately for each composite brain metric. Unlike traditional repeated-measures GLM approaches, HLM naturally handles the nested dependency and variable number of longitudinal assessments completed by each subject (Shiffman, Stone, & Hufford, 2008). Standardized (*z*-transformed) variables were used for all analyses. *Negative Affect* and *Stressors* (Level-1 variables) were nested within subjects. Intercepts were free to vary across subjects. *Brain* metrics served as continuous Level-2 predictors (grand-mean centered). For illustrative purposes, significant interactions are depicted for extreme values (±1 *SD*) of the relevant brain metric (Cohen, Cohen, West, & Aiken, 2003).

The following equations outline the basic structure of the HLMs in standard notation (Raudenbush & Bryk, 2002).

First, we examined relations between each brain metric and *tonic* (stressor-independent) negative affect ('NA'):

$$\boldsymbol{Eq.1a.}\ NA_{ti} = \pi_{0i} + e_{ti}$$

$$\boldsymbol{Eq.1b.}\ \pi_{0i} = \beta_{00} + \beta_{01}(Brain_i) + r_{0i}$$

Next, we probed the joint influence of each brain metric and momentary stressors on *reactive* (stessor-dependent) negative affect. At the first level, negative affect during EMA *t* for individual *i* was modeled as

a function of stressor exposure. The absence of stressor exposure served as the dummy-coded reference category (as in Equation 2a):

$$\boldsymbol{Eq.2a.}\ NA_{ti} = \pi_{0i} + \pi_{1i}(Stressor) + e_{ti}$$

At the second level, relations between stressors and negative affect was modeled as a function of each brain metric:

$$\boldsymbol{Eq.\ 2b.}\ \pi_{0i} = \beta_{00} + \beta_{01}(Brain_i) + r_{0i}$$

$$\boldsymbol{Eq.2c.}\ \pi_{1i} = \beta_{10} + \beta_{11}(Brain_i) + r_{1i}$$

For hypothesis testing purposes, a single model—incorporating terms for tonic *and* reactive negative affect—was implemented for each of the composite brain metrics. To further mitigate familywise alpha inflation, we used the Šidák procedure to determine corrected two-tailed significance thresholds for each hypothesis test (e.g. relations between brain activity and tonic negative affect) that included metrics derived from the anxiety-provocation paradigm (i.e., controlling for the two regional tests; Šidák, 1967).

Using the same general approach, follow-up analyses enabled us to determine whether significant brain-EMA associations generalize to positive affect and positive events, which would suggest a broader functional role. To gauge the added explanatory value ('incremental validity') of significant brain metrics, we re-computed the relevant HLM after incorporating an alternative brain metric (e.g., amygdala reactivity to threat-related faces) or our multi-occasion index of trait negative emotionality (conceptually similar to multiple regression). Finally, to enhance interpretability, we decomposed significant brain-EMA associations by performing follow-up analyses for the anxious and depressed facets of negative affect, and for the brain regions (e.g., MCC) incorporated into the focal composite.

Neurosynth. Neurosynth—a cloud-based suite of neuroinformatics tools and databases—was used to clarify the functional architecture of regions highlighted by the Brain-EMA results (Yarkoni, Poldrack, Nichols, Van Essen, & Wager, 2011). ***Functional connectivity.*** Regional intrinsic ('resting') functional connectivity was assessed using an automated seed-based approach and data from the Yeo-Buckner database, which incorporates fMRI data from 1,000 participants (Yeo et al., 2011). For illustrative purposes, connectivity maps were arbitrarily thresholded at a conservative level ($p < 1.76 \times 10^{-10}$, uncorrected). ***Meta-analytic co-activation.*** Regional co-activation patterns were meta-analytically assessed using an automated seed-based approach and a database of >500,000 stereotactic coordinates from >14,000 published imaging studies. Meta-analytic co-activation maps were thresholded using FDR $q < .01$ (whole-brain corrected).

RESULTS

As a precursor to hypothesis testing, we first confirmed that the anxiety-provocation and threat-related faces had the intended effects on behavior and brain function. As expected, waiting to receive aversive stimulation was associated with robust increases in subjective symptoms of distress (in-scanner ratings of fear and anxiety) and objective signs of arousal (skin conductance), *t*s(219)>27.00, *p*s<0.001 (**Figures 2a-b**). As shown in **Figure 2c** and detailed in **Supplementary Table S1**, voxelwise GLMs focused on the period of threat anticipation revealed significantly increased activity in key *subcortical* (dorsal amygdala, BST, PAG) and *frontocortical* regions (MCC; FrO; AI; and dlPFC extending into the frontal pole, FP) of the threat-anticipation network (FDR q<.05, whole-brain corrected; Hur et al., 2020b; Shackman & Fox, 2021). Likewise, the presentation of threat-related faces was associated with increased activity in the dorsal amygdala (**Figure 2d**), fusiform gyrus, and other regions of the ventral visual cortex (**Supplementary Table S2**).

To fuse the fMRI and EMA data-streams, we first extracted measures of task-related activation (i.e., regression coefficients) from ROIs centered on peak voxels in key anatomical regions for each task and subject (*asterisks* in **Figure 2**; see **Supplementary Tables S1-2** for coordinates). To reduce the number of comparisons, a factor analysis was used to guide the construction of composite measures for the anxiety-provocation task. Results revealed two latent factors, with subcortical ROIs (dorsal amygdala, BST, and PAG) loading on one factor and frontocortical ROIs (MCC, AI, FrO, and dlPFC/FP) loading on the other (**Supplementary Table S3**). Based on this, we standardized and averaged the ROI values to create composite measures of subcortical (α = .85) and frontocortical (α = .89) activation for each subject. A similar approach was used to create an amygdala composite for the threat-related faces task (α = .82). As shown schematically in **Figure 1**, a series of HLMs was then used to test relations between individual differences in task-related activation and momentary levels of *tonic* (stressor-independent) and *reactive* (stressor-dependent) negative affect. Unlike traditional repeated-measures GLM approaches, HLM naturally handles the nested dependency and variable number of EMAs completed by each subject (Shiffman et al., 2008).

We first examined the anxiety-provocation task. As shown in **Figure 3a** and **Table 1**, subcortical and frontocortical activation during the anticipation of threat was unrelated to tonic (stressor-independent) levels of negative affect (*p*s > .64). As expected, exposure to recent stressors was associated with elevated levels of negative affect (*p*s < .001). Subcortical reactivity was unrelated to the intensity of this stressor-dependent distress (p = .43). In contrast, frontocortical reactivity *was* significantly related (β = -.07, SE = .03, p = .02), and relations remained significant after applying a principled correction for the number of ROIs examined (Šidák $\alpha_{Critical}$ = .025). Closer inspection indicated that individuals showing *more* activation in frontocortical regions when anticipating aversive stimulation experienced *lower* levels of negative affect in the moments following stressor exposure, consistent with a regulatory role (**Figure 3a,**

inset). This association remained significant after controlling for individual differences in subcortical reactivity (β = -.09, p = .02; **Supplementary Table S4**), and similar effects were evident for both the anxious and depressed facets of the negative affect scale (βs = -.07, ps = .04-.05; **Supplementary Table S5**). Follow-up analyses indicated that frontocortical reactivity was unrelated to the frequency of momentary stressors (r = -.01, p = .91), and relations between frontocortical activity and reactive distress remained significant after controlling for individual differences in the frequency of stressor exposure (β = -.07, p = .02; **Supplementary Table S6**).

Next, we examined the emotional faces task. Variation in amygdala reactivity to threat-related faces was unrelated to tonic and reactive negative affect in the field (ps > .17; **Figure 3c** and **Table 1**). Consistent with this, relations between frontocortical reactivity to the threat-anticipation task and reactive negative affect remained significant after controlling for amygdala reactivity to faces, underscoring the unique explanatory contribution of frontocortical reactivity to the anxiety-provocation task (β = -.07, p = .03; **Supplementary Table S7**).

The present results show that heightened frontocortical activation while waiting for aversive stimulation is associated with lower levels of negative affect following exposure to everyday stressors, which is consistent with either a narrow role in dampening distress or a broader role in regulating emotion. To address this ambiguity, we used HLM to perform a parallel analysis for positive affect and positive events. Results indicated that frontocortical activation was unrelated to tonic or reactive positive affect, consistent with a narrower regulatory function (ps > .14; **Supplementary Table S8**).

In head-to-head comparisons of criterion validity, simple paper-and-pencil measures often outperform more sophisticated brain imaging measures (Shackman & Fox, 2018; Whelan et al., 2014). To clarify the explanatory value of frontocortical activation, we computed a new HLM that used a combination of

frontocortical reactivity *and* a multi-scale, multi-occasion composite measure of trait negative emotionality (see Method) to explain momentary negative affect (conceptually akin to a multiple regression). As expected, negativity emotionality promoted distress; individuals with a more negative temperament experienced higher levels of tonic *and* reactive negative affect in their daily lives (*p*s < .001) (Bolger, 1990; Bolger & Schilling, 1991; Gross et al., 1998; Shackman et al., 2016; Thake & Zelenski, 2013). But more importantly, relations between frontocortical activation and reactive (stressor-dependent) negative affect remained significant after controlling for trait-like individual differences in negative emotionality (β = -.06, p = .03; **Supplementary Table S9**). In other words, frontocortical reactivity to the anxiety-provocation task explained variation in daily distress above-and-beyond that accounted for by paper-and-pencil measures of emotional reactivity, underscoring the added explanatory value ('incremental validity') of the neuroimaging metric.

Multiregion composites offer a number of psychometric and statistical advantages, but, by their nature, do not address the contributions of the constituent regions. To address this, we used a series of HLMs to decompose the frontocortical composite and determine the relevance of individual regions to momentary negative affect. As shown in **Figure 4** and detailed in **Supplementary Table S10**, individuals showing greater activation in either the MCC or FrO during the threat-anticipation task experienced significantly lower levels of negative affect in the moments following stressor exposure in the field (*p*s < .01). Both associations remained significant after correcting for the number of ROIs examined (Šidák $\alpha_{Critical}$ = .013). None of the other brain-EMA effects was significant (*p*s > .11).

The present results raise the possibility that the MCC and FrO represent a coherent functional circuit. If so, then we would expect them to show robust functional connectivity 'at rest' (i.e. in the absence of an explicit task) *and* a consistent pattern of co-activation across experimental challenges (Laird et al., 2013; Yeo et al., 2011). We used Neurosynth—a cloud-based suite of neuroinformatics tools and databases—to

test these two predictions (Yarkoni et al., 2011). We began by assessing the intrinsic functional connectivity of the MCC and FrO in the Yeo-Buckner database (n = 1,000; Yeo et al., 2011), using the peak locations identified in the threat-anticipation task as seeds (cf. **Figure 2c**). In each case, there was substantial functional connectivity with the other seed locations (e.g., right MCC left FrO; $p < 1.76 \times 10^{-10}$, uncorrected; **Figure 5a**). We used a conceptually similar seed-based approach to probe MCC-FrO co-activation. This analysis leveraged a computer-generated database of >500,000 stereotactic coordinates derived from >14,000 published imaging studies. This allowed us to perform a series of automated meta-analyses, each quantifying the likelihood that activation in any one of the seed locations is associated with significant co-activation in the other three (FDR $q < .01$, whole-brain corrected). Mirroring the functional connectivity results, this revealed robust co-activation across the four seed locations (**Figure 5b**). Taken together, these results provide compelling evidence that the MCC and FrO form a cingulo-opercular circuit that is sensitive to threat-anticipation in the laboratory and associated with dampened stressor reactivity in daily life (**Figure 4**).

DISCUSSION

Anxiety, sadness, and other negative feelings are a hallmark of the human condition and play a central role in contemporary theories of decision making, development, interpersonal processes, personality, psychopathology, and well-being (Fox et al., 2018). Recent work has begun to reveal the neural systems governing the expression and regulation of negative affect, but the relevance of these tantalizing laboratory discoveries to the real world has remained uncertain. Here, we used a combination of fMRI and EMA data to demonstrate that individuals showing greater frontocortical activation during a well-established anxiety-provocation ('threat-anticipation') task experience dampened reactive (stressor-dependent) distress in their daily lives (**Figure 3**). Frontocortical activation was not significantly related to momentary positive affect or to tonic (stressor-independent) negative affect, suggesting a relatively narrow functional role. In a simultaneous HLM, frontocortical activation accounted for variation in daily

distress above-and-beyond a conventional psychometric measure of trait negative emotionality, underscoring its added explanatory value ('incremental validity'). Follow-up analyses indicated that this frontocortical association largely reflected heightened engagement of a functionally coherent cingulo-opercular (MCC and FrO) circuit (**Figures 4-5**).

These findings have implications for understanding the neural systems underlying negative affect. There is ample evidence that the MCC and FrO are recruited by distress-eliciting laboratory challenges, including instructed threat-of-shock, Pavlovian threat conditioning, and physical pain (Chavanne & Robinson, 2021; Fullana et al., 2016; Shackman et al., 2011; Xu et al., 2020). This has led some to conclude that the cingulo-opercular network plays a role in assembling and expressing negative affect (Etkin, Buchel, & Gross, 2015; Hinojosa, Kaur, VanElzakker, & Shin, 2019; Milad & Quirk, 2012). Yet recent meta-analyses make it clear that the MCC and FrO are also recruited by tasks that demand controlled processing and behavioral flexibility, including popular assays of cognitive conflict (e.g., go/no-go) and emotion regulation (Langner et al., 2018; Morawetz et al., 2020; Shackman et al., 2011; Uddin, *in press*). Other work shows that MCC activation tracks variation in both the cognitive demands associated with deliberate emotion regulation *and* the degree of regulatory success (Urry, van Reekum, Johnstone, & Davidson, 2009). The latter observations suggest that cingulo-opercular activation during aversive laboratory challenges actually reflects spontaneous efforts to down-regulate or inhibit distress, a negative-feedback-like process that some have termed 'implicit' emotion regulation (Shackman & Lapate, 2018; Van Reekum & Johnstone, 2018). Our results—which demonstrate that heightened cingulo-opercular reactivity to an anxiety provocation task is associated with lower levels of reactive (stressor-dependent) distress in the midst of daily life—are consistent with this hypothesis, and with evidence that surgical damage to the MCC ('cingulotomy') is associated with increased emotional reactivity to painful stimuli (Davis, Hutchison, Lozano, & Dostrovsky, 1994; Greenspan et al., 2008). They are also well aligned

with recent work showing that heightened cingulo-opercular reactivity to aversive images is associated with a greater likelihood of choosing to deliberately dampen reactivity when the same images are re-encountered outside the scanner (Doré et al., 2017). Together, this body of data is consistent with conceptual models that emphasize the importance of the cingulo-opercular network for flexibly controlling cognition, emotion, and action in situations where automatic or habitual responses are inadequate, as when there is competition between plausible alternative actions or between action and inaction (e.g., passively respond to emotional challenges vs. deliberately regulate the response) (Shackman et al., 2011; Uddin, *in press*). The present results help to extend this framework from the artificial confines of the neuroimaging laboratory to the real world.

Clearly, important challenges remain. First, the present study was focused on understanding the relevance of anxiety-related brain function to momentary levels of negative affect in the daily lives of young adults. Moving forward, it will be useful to expand this to encompass a broader range of ages and concurrent relations with trial-by-trial fluctuations in negative affect, an analytic approach not permitted by the sparse in-scanner ratings used here (Geuter et al., 2020; Lim, Padmala, & Pessoa, 2009). Second, our results indicate that subcortical reactivity to threat-anticipation and amygdala reactivity to threat-related faces in the laboratory are unrelated to distress in the field, despite a relatively well-powered sample. While there are a number of possible explanations, this null effect is not unprecedented. Three recent large-sample studies (Duke Neurogenetics Study: n = 1,256; HCP: n = 319; Minnesota Twin Study: n = 548) failed to detect credible relations between amygdala reactivity to threat-related faces and individual differences in negative emotionality (MacDuffie, Knodt, Radtke, Strauman, & Hariri, 2019; Silverman et al., 2019; West, Burgess, Dust, Kandala, & Barch, *in press*). Does this mean that the amygdala, BST, and PAG are unrelated to negative affect? No, mechanistic work in humans, monkeys, and rodents makes it abundantly clear that they are (Fox & Shackman, 2019; Hur et al., 2019). Instead, this work

raises the possibility that conventional fMRI measures of emotion perception (*viewing photographs of fearful or angry faces*) and generation (*briefly waiting for aversive stimulation*) are suboptimal probes of the aspects of subcortical function most relevant to everyday affect (i.e., 'wrong' assay) (Sicorello et al., 2021). Alternatively, it could be that isolated regional measures of subcortical function are only weakly predictive of conscious feelings of negative affect and, hence, to typical state, trait, and clinical assessments (Brown, Lau, & LeDoux, 2019; Chang et al., 2015; LeDoux & Pine, 2016; Shackman & Fox, 2018). Adjudicating between these possibilities is a key challenge for future research.

Anxiety disorders and depression are defined, diagnosed, and treated on the basis of negative feelings experienced in the midst of daily life. These disorders impose a staggering burden on global public health and existing treatments are inconsistently effective, underscoring the urgency of developing a deeper understanding of the underlying neurobiology (Dieleman et al., 2020; GBD 2019 Diseases and Injuries Collaborators, 2020; Ormel, Kessler, & Schoevers, 2019; Sartori & Singewald, 2019). The present findings highlight the relevance of cingulo-opercular function for real-world distress. These observations lay the groundwork for the kinds of prospective-longitudinal and mechanistic studies that will be necessary to determine causation and develop more effective interventions. A relatively large sample and best-practice approaches to data acquisition, processing, and analysis enhance confidence in the robustness and translational relevance of these results.

FIGURE LEGENDS

Figure 1. Overview of fMRI-EMA fusion. fMRI. All subjects were assessed using a well-established anxiety-provocation fMRI paradigm. On Threat trials, subjects saw a stream of integers that culminated with the delivery of a noxious electric shock, unpleasant photograph, and thematically related audio clip (e.g. growl, scream). Control trials were similar, but terminated with the delivery of benign reinforcers. A subset of subjects also completed a threat-related faces paradigm, during which they viewed photographs of fearful or angry faces. Photographs of neutral outdoor scenes served as a control. To facilitate integration of the fMRI and EMA data-streams, regions of interest were prescribed based on significant activation in whole-brain analyses (FDR $q < 0.05$, whole-brain corrected) within anatomical regions highlighted by prior work using similar tasks. For the anxiety-provocation task, analyses focused on *subcortical* (amygdala, BST, and PAG) and *frontocortical* (MCC, AI, FrO, and dlPFC) activation during the period of threat anticipation. To reduce the number of comparisons, factor analysis guided the construction of composite measures of brain activity. For the faces paradigm, analyses focused on a composite measure of bilateral amygdala activation. **EMA.** Smartphone EMA was used to sample hour-by-hour fluctuations in negative and positive affect. Subjects were also prompted to report exposure to stressors and positive events in the past hour, which allowed us to examine *tonic* (context-independent) and *reactive* (context-dependent) affect. Subjects completed up to 8 EMA surveys per day for 7 days, yielding a total of 10,239 usable assessments. **fMRI-EMA fusion.** A series of hierarchical linear models (HLMs) enabled us to selectively probe relations between the composite neuroimaging metrics derived from each task and tonic and reactive negative affect. A similar approach was used for follow-up analyses of specificity and incremental validity. Abbreviation—*e*, error (unmodeled variance); EMA, ecological momentary assessment; fMRI, functional magnetic resonance imaging; HLM, hierarchical linear modeling; *i*, intercept.

Figure 2. Anxiety-provocation (threat-anticipation) and threat-related faces paradigms considered in isolation. The anxiety-provocation paradigm produced robust symptoms (panel ***a***: in-scanner ratings) and signs (panel ***b***: skin conductance) of negative affect, confirming validity. Figures depict the data (dots and gray lines; *individual subjects*), density distribution (*bean plots*), Bayesian 95% highest density interval (HDI; *rectangular bands*), and mean (*bold black bars within the rectangular bands*) for each measure and condition. HDIs permit population-generalizable visual inferences about mean differences and were estimated using 1,000 samples from a posterior Gaussian distribution. The anxiety-provocation paradigm was also associated with increased activation (Threat > Safety; FDR q<.05, whole-brain corrected) in subcortical and frontocortical brain regions (panel ***c***). The presentation of threat-related faces was associated with increased activation in the dorsal amygdala (panel ***d***: Threat-Related Faces > Places; FDR q<.05, whole-brain corrected). Note: The amygdala and BST panels are masked to highlight suprathreshold voxels in the relevant regions. Black-and-white asterisks indicate the regions used for fMRI-EMA analyses (see the Method and **Supplementary Tables S1-S2** for details). Abbreviations—AI, anterior insula; BST, bed nucleus of the stria terminalis; dlPFC, dorsolateral prefrontal cortex; FP, frontal pole; FrO, frontal operculum; MCC, midcingulate cortex; PAG, periaqueductal grey; R, right; WB, whole-brain corrected.

Figure 3. **Frontocortical activation during the anxiety-provocation paradigm is associated with dampened reactive negative affect in the real world.** ***a.*** EMA-fMRI fusion for the anxiety-provocation paradigm. Figure depicts standardized HLM coefficients for EMA-derived measures of tonic (stressor-independent; *gray*) and reactive (stressor-dependent; *black*) negative affect. The left side of the panel depicts non-significant results for the subcortical composite. The right side depicts the results for the frontocortical composite. Error bars indicate the *SE*. Rendered brains depict the regions contributing to each composite (*gold*). Some regions are not visible. Inset depicts the decomposition of the Brain × Stressor interaction for the frontocortical composite. For illustrative purposes, HLM-predicted levels of negative affect are depicted for assessments associated with the absence (*orange*) or presence (*red*) of recent real-world stressors, separately for extreme levels (±1 *SD*) of frontocortical activation. Individuals with higher levels of frontocortical activation during the anxiety-provocation (threat-anticipation) in the laboratory experienced lower levels of negative affect in the moments following exposure to daily stressors. Hypothesis testing relied on continuous measures. ***b.*** EMA-fMRI fusion for the threat-related faces paradigm. Conventions are identical to panel *a*, and neither effect was significant. **Abbreviations**—AI, anterior insula; BST, bed nucleus of the stria terminalis; dlPFC, dorsolateral prefrontal cortex; FP, frontal pole; FrO, frontal operculum; MCC, midcingulate cortex; *n.s.,* not significant ($p > .05$); PAG, periaqueductal grey.

Figure 4. MCC and FrO reactivity to the anxiety-provocation paradigm is associated with dampened reactive negative affect in the real world. Conventions are identical to Figure 2a. ***a.*** MCC. ***b.*** FrO. ***c.*** AI. ***d.*** dlPFC/FP. **Abbreviations**—AI, anterior insula; dlPFC, dorsolateral prefrontal cortex; FP, frontal pole; FrO, frontal operculum; MCC, midcingulate cortex; *n.s.,* not significant ($p > .05$).

Figure 5. **The MCC and FrO form a coherent functional neuroanatomical circuit.** Asterisks depict the approximate location of each seed. **a. Functional connectivity.** Panel depicts the results of seed-based analyses of intrinsic functional connectivity between the MCC and FrO. Analyses were performed using Neurosynth and the Yeo-Buckner database of 1,000 'resting' fMRI assessments. See **Supplementary Table S1** for seed coordinates. Connectivity maps are shown using an arbitrary threshold ($p < 1.76 \times 10^{-10}$, uncorrected). **b. Co-activation.** Panel depicts the results of seed-based co-activation meta-analyses. Meta-analyses were automatically computed using the Neurosynth database, which encompasses peak coordinates from >15,000 published neuroimaging studies. Co-activation maps are depicted using a FDR $q < .01$, whole-brain corrected threshold. **Abbreviations**—FDR, false discovery rate; FrO, frontal operculum; *k*, the number of studies used in the meta-analysis; L, left; MCC, midcingulate cortex; WB, whole-brain corrected.

TABLE

Table 1. Relations between brain function in the laboratory and negative affect in the real world.

	Anxiety Provocation Subcortical[a] Composite			Anxiety Provocation Frontocortical[b] Composite			Threat-Related Faces Amygdala Composite		
	t	*β*	*SE*	*t*	*β*	*SE*	*t*	*β*	*SE*
Brain[c, d]	0.47	0.02	0.03	0.00	0.00	0.03	-0.48	-0.01	0.03
Stressor (vs. Absent)	14.93***	0.34	0.02	15.13***	0.34	0.02	14.85***	0.34	0.02
Brain[a] × Stressor	-.79	-0.02	0.03	-2.40*	-0.07	0.03	-1.36	-0.03	0.02

[a] Bilateral dorsal amygdala, bilateral BST, and PAG. [b] Bilateral MCC, FrO, AI, and dlPFC/FP. [c] Focal neural composite. The *Brain* term tests relations between neural function and tonic (stressor-independent) negative affect. The *Brain × Stressor* term tests relations between neural function and reactive (stressor-dependent) negative affect. [d] The same pattern of null results was evident in models that omitted the Stressor and Brain × Stressor terms (not shown). * $p \leq 0.05$, ** $p < 0.01$, *** $p < 0.001$

REFERENCES

Acosta-Cabronero, J., Williams, G. B., Pereira, J. M., Pengas, G., & Nestor, P. J. (2008). The impact of skull-stripping and radio-frequency bias correction on grey-matter segmentation for voxel-based morphometry. *Neuroimage, 39*, 1654-1665.

Albaugh, M. D., Hudziak, J. J., Orr, C., Spechler, P. A., Chaarani, B., Mackey, S., . . . Consortium, I. (2019). Amygdalar reactivity is associated with prefrontal cortical thickness in a large population-based sample of adolescents. *PLoS One, 14*, e0216152.

Allen, M., Poggiali, D., Whitaker, K., Marshall, T., & Kievit, R. A. (2019). Raincloud plots: a multi-platform tool for robust data visualization. *Wellcome Open Research, 4*.

Amunts, K., Lenzen, M., Friederici, A. D., Schleicher, A., Morosan, P., Palomero-Gallagher, N., & Zilles, K. (2010). Broca's region: novel organizational principles and multiple receptor mapping. *PLoS biology, 8*, e1000489.

Andersson, J. L. R., Skare, S., & Ashburner, J. (2003). How to correct susceptibility distortions in spin-echo echo-planar images: application to diffusion tensor imaging. *Neuroimage, 20*, 870-888.

Avants, B. B., Tustison, N. J., Song, G., Cook, P. A., Klein, A., & Gee, J. C. (2011). A reproducible evaluation of ANTs similarity metric performance in brain image registration. *Neuroimage, 54*, 2033-2044.

Bach, D. R. (2014). A head-to-head comparison of SCRalyze and Ledalab, two model-based methods for skin conductance analysis. *Biol Psychol, 103*, 63-68.

Bach, D. R., Castegnetti, G., Korn, C. W., Gerster, S., Melinscak, F., & Moser, T. (2018). Psychophysiological modeling: Current state and future directions. *Psychophysiology, 55*, e13214.

Bach, D. R., Flandin, G., Friston, K. J., & Dolan, R. J. (2009). Time-series analysis for rapid event-related skin conductance responses. *J Neurosci Methods, 184*, 224-234.

Bach, D. R., Flandin, G., Friston, K. J., & Dolan, R. J. (2010). Modelling event-related skin conductance responses. *Int J Psychophysiol, 75*, 349-356.

Bach, D. R., & Friston, K. J. (2013). Model-based analysis of skin conductance responses: Towards causal models in psychophysiology. *Psychophysiology, 50*, 15-22.

Bach, D. R., Friston, K. J., & Dolan, R. J. (2013). An improved algorithm for model-based analysis of evoked skin conductance responses. *Biol Psychol, 94*, 490-497.

Barch, D. M., Burgess, G. C., Harms, M. P., Petersen, S. E., Schlaggar, B. L., Corbetta, M., . . . Consortium, W. U.-M. H. (2013). Function in the human connectome: task-fMRI and individual differences in behavior. *Neuroimage, 80*, 169-189.

Bijsterbosch, J., Harrison, S. J., Jbabdi, S., Woolrich, M., Beckmann, C., Smith, S., & Duff, E. P. (2020). Challenges and future directions for representations of functional brain organization. *Nature Neuroscience, 23*, 1484-1495.

Bolger, N. (1990). Coping as a personality process: a prospective study. *J Pers Soc Psychol, 59*, 525-537.

Bolger, N., & Schilling, E. A. (1991). Personality and the problems of everyday life: the role of neuroticism in exposure and reactivity to daily stressors. *J Pers, 59*, 355-386.

Brown, R., Lau, H., & LeDoux, J. E. (2019). Understanding the higher-order approach to consciousness. *Trends in cognitive sciences, 23*, 754-768.

Casey, B. J., Cannonier, T., Conley, M. I., Cohen, A. O., Barch, D. M., Heitzeg, M. M., . . . Workgroup, A. I. A. (2018). The Adolescent Brain Cognitive Development (ABCD) study: Imaging acquisition across 21 sites. *Dev Cogn Neurosci, 32*, 43-54.

Chang, L. J., Gianaros, P. J., Manuck, S. B., Krishnan, A., & Wager, T. D. (2015). A sensitive and specific neural signature for picture-induced negative affect. *PLoS biology, 13*, e1002180.

Chavanne, A. V., & Robinson, O. J. (2021). The overlapping neurobiology of adaptive and pathological anxiety: a meta-analysis of functional neural activation. *American Journal of Psychiatry, 178*, 156-164.

Choi, J. M., Padmala, S., & Pessoa, L. (2012). Impact of state anxiety on the interaction between threat monitoring and cognition. *NeuroImage, 59*(2), 1912-1923.

Choi, J. M., Padmala, S., & Pessoa, L. (2015). Counteracting effect of threat on reward enhancements during working memory. *Cognition and Emotion, 29*(8), 1517-1526.

Cohen, J., Cohen, P., West, S. G., & Aiken, L. S. (2003). *Applied multiple regression/correlation analysis for the behavioral sciences* (3rd ed.). Mahwah, NJ: LEA.

Cox, R. W. (1996). AFNI: Software for analysis and visualization of functional magnetic resonance neuroimages. *Computers and Biomedical Research, 29*, 162-173.

Cox, R. W., Jesmanowicz, A., & Hyde, J. S. (1995). Real-time functional magnetic resonance imaging. *Magn Reson Med, 33*, 230-236.

Davis, K. D., Hutchison, W. D., Lozano, A. M., & Dostrovsky, J. O. (1994). Altered pain and temperature perception following cingulotomy and capsulotomy in a patient with schizoaffective disorder. *Pain, 59*, 189-199.

Desikan, R. S., Ségonne, F., Fischl, B., Quinn, B. T., Dickerson, B. C., Blacker, D., . . . Killiany, R. J. (2006). An automated labeling system for subdividing the human cerebral cortex on MRI scans into gyral based regions of interest. *Neuroimage, 31*, 968-980.

Dieleman, J. L., Cao, J., Chapin, A., Chen, C., Li, Z., Liu, A., . . . Murray, C. J. L. (2020). US health care spending by payer and health condition, 1996-2016. *JAMA, 323*, 863-884.

Doorley, J. D., Goodman, F. R., Disabato, D. J., Kashdan, T. B., Weinstein, J. S., & Shackman, A. J. (*in press*). The momentary benefits of positive events for individuals with elevated social anxiety. *Emotion*.

Doorley, J. D., Volgenau, K. M., Kelso, K. C., Kashdan, T. B., & Shackman, A. J. (2020). Do people with elevated social anxiety respond differently to digital and face-to-face communications? Two daily diary studies with null effects *Journal of Affective Disorders, 276*, 859-865.

Doré, B. P., Weber, J., & Ochsner, K. N. (2017). Neural predictors of decisions to cognitively control emotion. *J Neurosci, 37*, 2580-2588.

Ebner, N. C., Riediger, M., & Lindenberger, U. (2010). FACES—A database of facial expressions in young, middle-aged, and older women and men: Development and validation. *Behavior research methods, 42*(1), 351-362.

Ekman, P., & Friesen, W. (1976). Pictures of Facial Affect (Palo Alto, CA: Consulting Psychologists).

Elliott, M. L., Knodt, A. R., Ireland, D., Morris, M. L., Poulton, R., Ramrakha, S., . . . Hariri, A. R. (2019). Poor test-retest reliability of task-fMRI: New empirical evidence and a meta-analysis. *bioRxiv*, 681700.

Eskildsen, S. F., Coupé, P., Fonov, V., Manjón, J. V., Leung, K. K., Guizard, N., . . . Alzheimer's Disease Neuroimaging Initiative. (2012). BEaST: brain extraction based on nonlocal segmentation technique. *Neuroimage, 59*, 2362-2373.

Etkin, A., Buchel, C., & Gross, J. J. (2015). The neural bases of emotion regulation. *Nat Rev Neurosci, 16*, 693-700.

Fein, G., Landman, B., Tran, H., Barakos, J., Moon, K., Di Sclafani, V., & Shumway, R. (2006). Statistical parametric mapping of brain morphology: sensitivity is dramatically increased by using brain-extracted images as inputs. *Neuroimage, 30*, 1187-1195.

First, M. B., Williams, J. B. W., Karg, R. S., & Spitzer, R. L. (2015). Structured clinical interview for DSM-5—Research version (SCID-5 for DSM-5, research version; SCID-5-RV). *Arlington, VA: American Psychiatric Association*.

Fischmeister, F. P., Hollinger, I., Klinger, N., Geissler, A., Wurnig, M. C., Matt, E., . . . Beisteiner, R. (2013). The benefits of skull stripping in the normalization of clinical fMRI data. *Neuroimage Clin, 3*, 369-380.

Fox, A. S., Lapate, R. C., Shackman, A. J., & Davidson, R. J. (2018). *The nature of emotion. Fundamental questions* (2nd ed.). New York, NY: Oxford University Press.

Fox, A. S., Oler, J. A., Shackman, A. J., Shelton, S. E., Raveendran, M., McKay, D. R., . . . Kalin, N. H. (2015). Intergenerational neural mediators of early-life anxious temperament. *Proceedings of the National Academy of Sciences USA, 112*, 9118-9122.

Fox, A. S., & Shackman, A. J. (2019). The central extended amygdala in fear and anxiety: Closing the gap between mechanistic and neuroimaging research. *Neuroscience letters, 693*, 58-67.

Frazier, J. A., Chiu, S., Breeze, J. L., Makris, N., Lange, N., Kennedy, D. N., . . . Biederman, J. (2005). Structural brain magnetic resonance imaging of limbic and thalamic volumes in pediatric bipolar disorder. *American Journal of Psychiatry, 162*, 1256-1265.

Fullana, M. A., Harrison, B. J., Soriano-Mas, C., Vervliet, B., Cardoner, N., Àvila-Parcet, A., & Radua, J. (2016). Neural signatures of human fear conditioning: An updated and extended meta-analysis of fMRI studies. *Molecular Psychiatry, 21*, 500-508.

Gamer, M., Schmitz, A. K., Tittgemeyer, M., & Schilbach, L. (2013). The human amygdala drives reflexive orienting towards facial features. *Current Biology, 23*(20), R917-R918.

GBD 2019 Diseases and Injuries Collaborators. (2020). Global burden of 369 diseases and injuries in 204 countries and territories, 1990-2019: a systematic analysis for the Global Burden of Disease Study 2019. *The Lancet, 396*(10258), 1204-1222. (interactive dashboard at https://vizhub.healthdata.org/gbd-compare/).

Gerster, S., Namer, B., Elam, M., & Bach, D. R. (2018). Testing a linear time invariant model for skin conductance responses by intraneural recording and stimulation. *Psychophysiology, 55*.

Geuter, S., Reynolds Losin, E. A., Roy, M., Atlas, L. Y., Schmidt, L., Krishnan, A., . . . Lindquist, M. A. (2020). Multiple brain networks mediating stimulus–pain relationships in humans. *Cerebral Cortex, 30*, 4204-4219.

Goldberg, L. R. (1999). A broad-bandwidth, public domain, personality inventory measuring the lower-level facets of several five-factor models. In I. Mervielde, I. Deary, F. De Fruyt, & F. Ostendorf (Eds.), *Personality Psychology in Europe* (Vol. 7, pp. 7-28). Tilburg, The Netherlands: Tilburg University Press.

Goldberg, L. R., Johnson, J. A., Eber, H. W., Hogan, R., Ashton, M. C., Cloninger, C. R., & Gough, H. C. (2006). The International Personality Item Pool and the future of public-domain personality measures. *Journal of Research in Personality, 40*, 84-96.

Grabner, G., Janke, A. L., Budge, M. M., Smith, D., Pruessner, J., & Collins, D. L. (2006). Symmetric atlasing and model based segmentation: an application to the hippocampus in older adults. *Med Image Comput Comput Assist Interv Int Conf Med Image Comput Comput Assist Interv, 9*, 58–66.

Graham, M. S., Drobnjak, I., & Zhang, H. (2017). Quantitative assessment of the susceptibility artefact and its interaction with motion in diffusion MRI. *PLoS One, 12*, e0185647.

Greenspan, J. D., Coghill, R. C., Gilron, I., Sarlani, E., Veldhuijzen, D. S., & Lenz, F. A. (2008). Quantitative somatic sensory testing and functional imaging of the response to painful stimuli before and after cingulotomy for obsessive-compulsive disorder (OCD). *European Journal of Pain, 12*, 990-999.

Greve, D. N., & Fischl, B. (2009). Accurate and robust brain image alignment using boundary-based registration. *Neuroimage, 48*, 63-72.

Gross, J. J., Sutton, S. K., & Ketelaar, T. (1998). Relations between affect and personality: Support for the affect-level and affective reactivity views. *Personality and Social Psychology Bulletin, 24*, 279-288.

Hauner, K. K., Zinbarg, R. E., & Revelle, W. (2014). A latent variable model approach to estimating systematic bias in the oversampling method. *Behav Res, 46*, 786-797.

Hawrylycz, M. J., Lein, E. S., Guillozet-Bongaarts, A. L., Shen, E. H., Ng, L., Miller, J. A., . . . Jones, A. R. (2012). An anatomically comprehensive atlas of the adult human brain transcriptome. *Nature, 489*, 391-399.

Henson, R. (2007a). Efficient experimental design for fMRI. In K. Friston, J. Ashburner, S. Kiebel, T. Nichols, & W. Penny (Eds.), *Statistical parametric mapping: The analysis of functional brain images* (pp. 193-210). New York, NY: Academic Press.

Henson, R. (2007b). Efficient experimental design for fMRI. *Statistical parametric mapping: The analysis of functional brain images*, 193-210.

Hinojosa, C. A., Kaur, N., VanElzakker, M. B., & Shin, L. M. (2019). Cingulate subregions in posttraumatic stress disorder, chronic stress, and treatment. In B. A. Vogt (Ed.), *Handbook of Clinical Neurology* (Vol. 166, pp. 355-370). New York, NY: Elsevier.

Hofmann, W., & Patel, P. V. (2015). SurveySignal. A convenient solution for experience sampling research using participants' own smartphones. *Social Science Computer Review, 33*, 235-253.

Horikawa, T., Cowen, A. S., Keltner, D., & Kamitani, Y. (2020). The neural representation of visually evoked emotion Is high-dimensional, categorical, and distributed across transmodal brain regions. *iScience, 23*, 101060.

Hur, J., DeYoung, K. A., Islam, S., Anderson, A. S., Barstead, M. G., & Shackman, A. J. (2020a). Social context and the real-world consequences of social anxiety. *Psychological Medicine, 50*, 1989-2000.

Hur, J., Kaplan, C. M., Smith, J. F., Bradford, D. E., Fox, A. S., Curtin, J. J., & Shackman, A. J. (2018). Acute alcohol administration dampens central extended amygdala reactivity. *Scientific Reports, 8*, 16702.

Hur, J., Smith, J. F., DeYoung, K. A., Anderson, A. S., Kuang, J., Kim, H. C., . . . Shackman, A. J. (2020b). Anxiety and the neurobiology of temporally uncertain threat anticipation. *Journal of Neuroscience, 40*, 7949-7964.

Hur, J., Stockbridge, M. D., Fox, A. S., & Shackman, A. J. (2019). Dispositional negativity, cognition, and anxiety disorders: An integrative translational neuroscience framework. *Progress in Brain Research, 247*, 375-436.

Jo, H. J., Gotts, S. J., Reynolds, R. C., Bandettini, P. A., Martin, A., Cox, R. W., & Saad, Z. S. (2013). Effective preprocessing procedures virtually eliminate distance-dependent motion artifacts in resting state FMRI. *Journal of Applied Mathematics, 2013*, 1-9.

John, O. P., Naumann, L. P., & Soto, C. J. (2008). Paradigm shift to the integrative big-five trait taxonomy: History, measurement, and conceptual issues. In O. P. John, R. W. Robins, & L. A. Pervin (Eds.), *Handbook of personality: Theory and research* (pp. 114-158). NY: Guilford.

Kenwood, M. M., & Kalin, N. H. (2021). Nonhuman primate models to explore mechanisms underlying early-life temperamental anxiety. *Biological Psychiatry, 89*, 659-671.

Klein, A., Andersson, J., Ardekani, B. A., Ashburner, J., Avants, B., Chiang, M. C., . . . Parsey, R. V. (2009). Evaluation of 14 nonlinear deformation algorithms applied to human brain MRI registration. *Neuroimage, 46*, 786-802.

Laird, A. R., Eickhoff, S. B., Rottschy, C., Bzdok, D., Ray, K. L., & Fox, P. T. (2013). Networks of task co-activations. *Neuroimage, 80*, 505-514.

Langner, R., Leiberg, S., Hoffstaedter, F., & Eickhoff, S. B. (2018). Towards a human self-regulation system: Common and distinct neural signatures of emotional and behavioural control. *Neurosci Biobehav Rev, 90*, 400-410.

LeDoux, J. E., & Pine, D. S. (2016). Using neuroscience to help understand fear and anxiety: A two-system framework. *Am J Psychiatry, 173*, 1083-1093.

Lim, S., & Jahng, S. (2019). Determining the number of factors using parallel analysis and its recent variants. *Psychol Methods, 24*, 452-467.

Lim, S. L., Padmala, S., & Pessoa, L. (2009). Segregating the significant from the mundane on a moment-to-moment basis via direct and indirect amygdala contributions. *Proc Natl Acad Sci U S A, 106*, 16841-16846.

Lopez, R. B., Chen, P.-H. A., Huckins, J. F., Hofmann, W., Kelley, W. M., & Heatherton, T. F. (2017). A balance of activity in brain control and reward systems predicts self-regulatory outcomes. *Social cognitive and affective neuroscience, 12*, 832-838.

Lopez, R. B., Hofmann, W., Wagner, D. D., Kelley, W. M., & Heatherton, T. F. (2014). Neural predictors of giving in to temptation in daily life. *Psychol Sci, 25*, 1337-1344.

Lorio, S., Fresard, S., Adaszewski, S., Kherif, F., Chowdhury, R., Frackowiak, R. S., . . . Draganski, B. (2016). New tissue priors for improved automated classification of subcortical brain structures on MRI. *Neuroimage, 130*, 157-166.

MacDuffie, K. E., Knodt, A. R., Radtke, S. R., Strauman, T. J., & Hariri, A. R. (2019). Self-rated amygdala activity: an auto-biological index of affective distress. *Personal Neurosci, 2*, e1.

Mai, J. K., Majtanik, M., & Paxinos, G. (2015). *Atlas of the human brain* (4th ed.). San Diego, CA: Academic Press.

Makris, N., Goldstein, J. M., Kennedy, D., Hodge, S. M., Caviness, V. S., Faraone, S. V., . . . Seidman, L. J. (2006). Decreased volume of left and total anterior insular lobule in schizophrenia. *Schizophrenia Research, 83*, 155-171.

Maus, B., van Breukelen, G. J., Goebel, R., & Berger, M. P. (2010). Optimization of blocked designs in fMRI studies. *Psychometrika, 75*(2), 373-390.

Milad, M. R., & Quirk, G. J. (2012). Fear extinction as a model for translational neuroscience: ten years of progress. *Annu Rev Psychol, 63*, 129-151.

Miller, K. L., Alfaro-Almagro, F., Bangerter, N. K., Thomas, D. L., Yacoub, E., Xu, J., . . . Smith, S. M. (2016). Multimodal population brain imaging in the UK Biobank prospective epidemiological study. *Nat Neurosci, 19*, 1523-1536.

Mobbs, D., Adolphs, R., Fanselow, M. S., Barrett, L. F., LeDoux, J. E., Ressler, K., & Tye, K. M. (2019). Viewpoints: Approaches to defining and investigating fear. *Nature Neuroscience, 22*, 1205-1216.

Moffitt, T. E., Arseneault, L., Belsky, D., Dickson, N., Hancox, R. J., Harrington, H., . . . Caspi, A. (2011). A gradient of childhood self-control predicts health, wealth, and public safety. *Proc Natl Acad Sci U S A, 108*, 2693-2698.

Morawetz, C., Riedel, M. C., Salo, T., Berboth, S., Eickhoff, S. B., Laird, A. R., & Kohn, N. (2020). Multiple large-scale neural networks underlying emotion regulation. *Neuroscience & Biobehavioral Reviews, 116*, 382-395.

Mõttus, R., Wood, D., Condon, D. M., Back, M. D., Baumert, A., Costantini, G., . . . Zimmermann, J. (2020). Descriptive, predictive and explanatory personality research: Different goals, different

approaches, but a shared need to move beyond the Big Few traits. *European Journal of Personality, 34*, 1175-1201.

National Academies of Sciences, Engineering, & Medicine. (2021). *Mental health, substance use, and wellbeing in higher education: Supporting the whole student*. Washington, DC: The National Academies Press.

Ormel, J., Kessler, R. C., & Schoevers, R. (2019). Depression: more treatment but no drop in prevalence: how effective is treatment? And can we do better? *Curr Opin Psychiatry, 32*, 348-354.

Palmier-Claus, J. E., Myin-Germeys, I., Barkus, E., Bentley, L., Udachina, A., Delespaul, P. A., . . . Dunn, G. (2011). Experience sampling research in individuals with mental illness: reflections and guidance. *Acta Psychiatr Scand, 123*(1), 12-20.

Plichta, M. M., Grimm, O., Morgen, K., Mier, D., Sauer, C., Haddad, L., . . . Schwarz, A. J. (2014). Amygdala habituation: a reliable fMRI phenotype. *Neuroimage, 103*, 383-390.

Poldrack, R. A., Baker, C. I., Durnez, J., Gorgolewski, K. J., Matthews, P. M., Munafo, M. R., . . . Yarkoni, T. (2017). Scanning the horizon: towards transparent and reproducible neuroimaging research. *Nat Rev Neurosci, 18*, 115-126.

Power, J. D., Schlaggar, B. L., & Petersen, S. E. (2015). Recent progress and outstanding issues in motion correction in resting state fMRI. *Neuroimage, 105*, 536-551.

Pruim, R. H. R., Mennes, M., van Rooij, D., Llera, A., Buitelaar, J. K., & Beckmann, C. F. (2015). ICA-AROMA: a robust ICA-based strategy for removing motion artifacts from fMRI data. *Neuroimage, 112*, 267-277.

Raudenbush, S. W., & Bryk, A. S. (2002). *Hierarchical linear models. Applications and data analysis methods* (2nd ed.). Thousand Oakes, CA: Sage.

Sartori, S. B., & Singewald, N. (2019). Novel pharmacological targets in drug development for the treatment of anxiety and anxiety-related disorders. *Pharmacology & Therapeutics, 204*, 107402.

Satterthwaite, T. D., Connolly, J. J., Ruparel, K., Calkins, M. E., Jackson, C., Elliott, M. A., . . . Gur, R. E. (2016). The Philadelphia Neurodevelopmental Cohort: A publicly available resource for the study of normal and abnormal brain development in youth. *Neuroimage, 124*, 1115-1119.

Scheller, E., Büchel, C., & Gamer, M. (2012). Diagnostic features of emotional expressions are processed preferentially. *PLoS One, 7*(7), e41792.

Schönbrodt, F. D., & Perugini, M. (2013). At what sample size do correlations stabilize? *Journal of Research in Personality, 47*, 609–612.

Seok, D., Smyk, N., Jaskir, M., Cook, P., Elliott, M., Girelli, T., . . . Sheline, Y. (2020). Dimensional connectomics of anxious misery, a human connectome study related to human disease: Overview of protocol and data quality. *NeuroImage: Clinical, 28*, 102489.

Shackman, A. J., & Fox, A. S. (2018). Getting serious about variation: Lessons for clinical neuroscience. *Trends in cognitive sciences, 22*, 368-369.

Shackman, A. J., & Fox, A. S. (2021). Two decades of anxiety neuroimaging research: New insights and a look to the future *American Journal of Psychiatry, 178*, 106-109.

Shackman, A. J., & Lapate, R. C. (2018). How are emotions regulated by context and cognition? In A. S. Fox, R. C. Lapate, A. J. Shackman, & R. J. Davidson (Eds.), *The nature of emotion. Fundamental questions* (2nd ed., pp. 177-179). New York, NY: Oxford University Press.

Shackman, A. J., Salomons, T. V., Slagter, H. A., Fox, A. S., Winter, J. J., & Davidson, R. J. (2011). The integration of negative affect, pain and cognitive control in the cingulate cortex. *Nat Rev Neurosci, 12*, 154-167.

Shackman, A. J., Tromp, D. P. M., Stockbridge, M. D., Kaplan, C. M., Tillman, R. M., & Fox, A. S. (2016). Dispositional negativity: An integrative psychological and neurobiological perspective. *Psychological Bulletin, 142*, 1275-1314.

Shackman, A. J., Weinstein, J. S., Hudja, S. N., Bloomer, C. D., Barstead, M. G., Fox, A. S., & Lemay, E. P., Jr. (2018). Dispositional negativity in the wild: Social environment governs momentary emotional experience. *Emotion, 18*, 707-724.

Shiffman, S., Stone, A. A., & Hufford, M. R. (2008). Ecological momentary assessment. *Annu Rev Clin Psychol, 4*, 1-32.

Sicorello, M., Herzog, J., Wager, T. D., Ende, G., Mueller-Engelmann, M., Herpertz, S. C., . . . Niedtfeld, I. (2021). Affective neural signatures do not distinguish women with emotion dysregulation from healthy controls: A mega-analysis across three task-based fMRI studies. *medRxiv*, 2021.2002.2003.21251077.

Šidák, Z. (1967). Rectangular confidence regions for the means of multivariate normal distributions. *Journal of the American Statistical Association, 62*, 626-633.

Siegel, J. S., Power, J. D., Dubis, J. W., Vogel, A. C., Church, J. A., Schlaggar, B. L., & Petersen, S. E. (2014). Statistical improvements in functional magnetic resonance imaging analyses produced by censoring high-motion data points. *Human Brain Mapping, 35*, 1981-1996.

Siless, V., Hubbard, N. A., Jones, R., Wang, J., Lo, N., Bauer, C. C. C., . . . Yendiki, A. (2020). Image acquisition and quality assurance in the Boston Adolescent Neuroimaging of Depression and Anxiety study. *Neuroimage Clin, 26*, 102242.

Silverman, M. H., Wilson, S., Ramsay, I. S., Hunt, R. H., Thomas, K. M., Krueger, R. F., & Iacono, W. G. (2019). Trait neuroticism and emotion neurocircuitry: Functional magnetic resonance imaging evidence for a failure in emotion regulation. *Development and Psychopathology, 31*, 1085-1099.

Smith, S. M., Jenkinson, M., Woolrich, M. W., Beckmann, C. F., Behrens, T. E. J., Johansen-Berg, H., . . . Matthews, P. M. (2004). Advances in functional and structural MR image analysis and implementation as FSL. *Neuroimage, 23(S1)*, 208-219.

Somerville, L. H., Bookheimer, S. Y., Buckner, R. L., Burgess, G. C., Curtiss, S. W., Dapretto, M., . . . Barch, D. M. (2018). The Lifespan Human Connectome Project in Development: A large-scale study of brain connectivity development in 5–21 year olds. *Neuroimage, 183*, 456-468.

Substance Abuse and Mental Health Services Administration. (2019). *Key substance use and mental health indicators in the United States: Results from the 2018 National Survey on Drug Use and Health*. Rockville, MD: Center for Behavioral Health Statistics and Quality.

Swartz, J. R., Knodt, A. R., Radtke, S. R., & Hariri, A. R. (2015). A neural biomarker of psychological vulnerability to future life stress. *Neuron, 85*, 505-511.

Taschereau-Dumouchel, V., Kawato, M., & Lau, H. (2019). Multivoxel pattern analysis reveals dissociations between subjective fear and its physiological correlates. *Molecular Psychiatry, 25*(2342-2354), 2342-2354.

ten Donkelaar, H. J., Tzourio-Mazoyer, N., & Mai, J. K. (2018). Toward a common terminology for the gyri and sulci of the human cerebral cortex. *Frontiers in Neuroanatomy, 12*.

Thake, J., & Zelenski, J. M. (2013). Neuroticism, BIS, and reactivity to discrete negative mood inductions. *Personality and Individual Differences, 54*, 208-213.

Tillman, R. M., Stockbridge, M. D., Nacewicz, B. M., Torrisi, S., Fox, A. S., Smith, J. F., & Shackman, A. J. (2018). Intrinsic functional connectivity of the central extended amygdala. *Human Brain Mapping, 39*, 1291-1312.

Tozzi, L., Staveland, B., Holt-Gosselin, B., Chesnut, M., Chang, S. E., Choi, D., . . . Williams, L. M. (2020). The human connectome project for disordered emotional states: Protocol and rationale for a research domain criteria study of brain connectivity in young adult anxiety and depression. *Neuroimage, 214*, 116715.

Tustison, N. J., Avants, B. B., Cook, P. A., Zheng, Y. J., Egan, A., Yushkevich, P. A., & Gee, J. C. (2010). N4ITK: Improved N3 bias correction. *IEEE Transactions on Medical Imaging, 29*, 1310-1320.

Tyszka, J. M., & Pauli, W. M. (2016). In vivo delineation of subdivisions of the human amygdaloid complex in a high-resolution group template. *Hum Brain Mapp, 37*, 3979-3998.

Uddin, L. Q. (*in press*). Cognitive and behavioural flexibility: neural mechanisms and clinical considerations. *Nature Reviews Neuroscience*.

Urry, H. L., van Reekum, C. M., Johnstone, T., & Davidson, R. J. (2009). Individual differences in some (but not all) medial prefrontal regions reflect cognitive demand while regulating unpleasant emotion. *Neuroimage, 47*, 852-863.

van Langen, J. (2020). Open-visualizations in R and Python (Version v.1.0.4). *Zenodo*.

Van Reekum, C. M., & Johnstone, T. (2018). Emotion regulation as a change of goals and priorities. In A. S. Fox, R. C. Lapate, A. J. Shackman, & R. J. Davidson (Eds.), *The nature of emotion. Fundamental questions.* (2nd ed., pp. 165-169). New York, NY: Oxford University Press.

West, H. V., Burgess, G. C., Dust, J., Kandala, S., & Barch, D. M. (*in press*). Amygdala activation in cognitive task fMRI varies with individual differences in cognitive traits. *Cognitive, Affective, & Behavioral Neuroscience*.

Whelan, R., Watts, R., Orr, C. A., Althoff, R. R., Artiges, E., Banaschewski, T., . . . Consortium, I. (2014). Neuropsychosocial profiles of current and future adolescent alcohol misusers. *Nature, 512*, 185-189.

Xu, A., Larsen, B., Baller, E. B., Scott, J. C., Sharma, V., Adebimpe, A., . . . Satterthwaite, T. D. (2020). Convergent neural representations of experimentally-induced acute pain in healthy volunteers: A large-scale fMRI meta-analysis. *Neurosci Biobehav Rev, 112*, 300-323.

Yarkoni, T., Poldrack, R. A., Nichols, T. E., Van Essen, D. C., & Wager, T. D. (2011). Large-scale automated synthesis of human functional neuroimaging data. *Nat Methods, 8*, 665-670.

Yeo, B. T., Krienen, F. M., Sepulcre, J., Sabuncu, M. R., Lashkari, D., Hollinshead, M., . . . Buckner, R. L. (2011). The organization of the human cerebral cortex estimated by intrinsic functional connectivity. *J Neurophysiol, 106*, 1125-1165.

Zhang, Y., Brady, M., & Smith, S. (2001). Segmentation of brain MR images through a hidden Markov random field model and the expectation-maximization algorithm. *IEEE Transactions in Medical Imaging, 20*, 45-57.

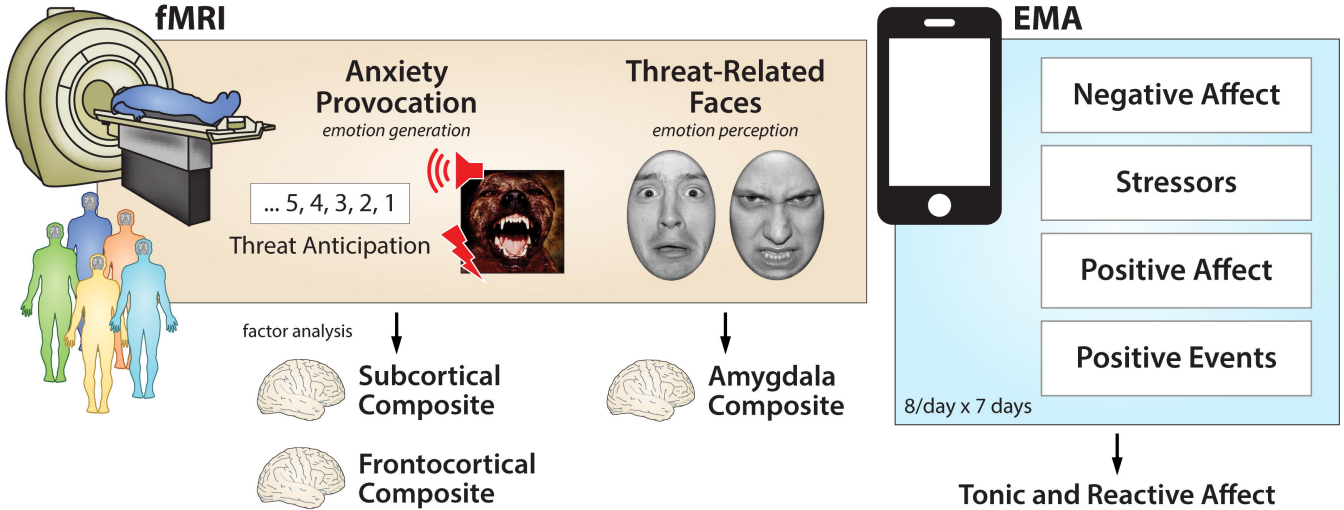

Using HLM, Negative Affect can be modeled as $\beta_i + \beta_{Brain} + \beta_{Stressor} + \beta_{Stressor\ x\ Brain} + e$

β_{Brain} — relations between brain function and *tonic* (stressor-independent) affect

$\beta_{Brain\ x\ Stressor}$ — relations between brain function and *reactive* (stressor-dependent) affect

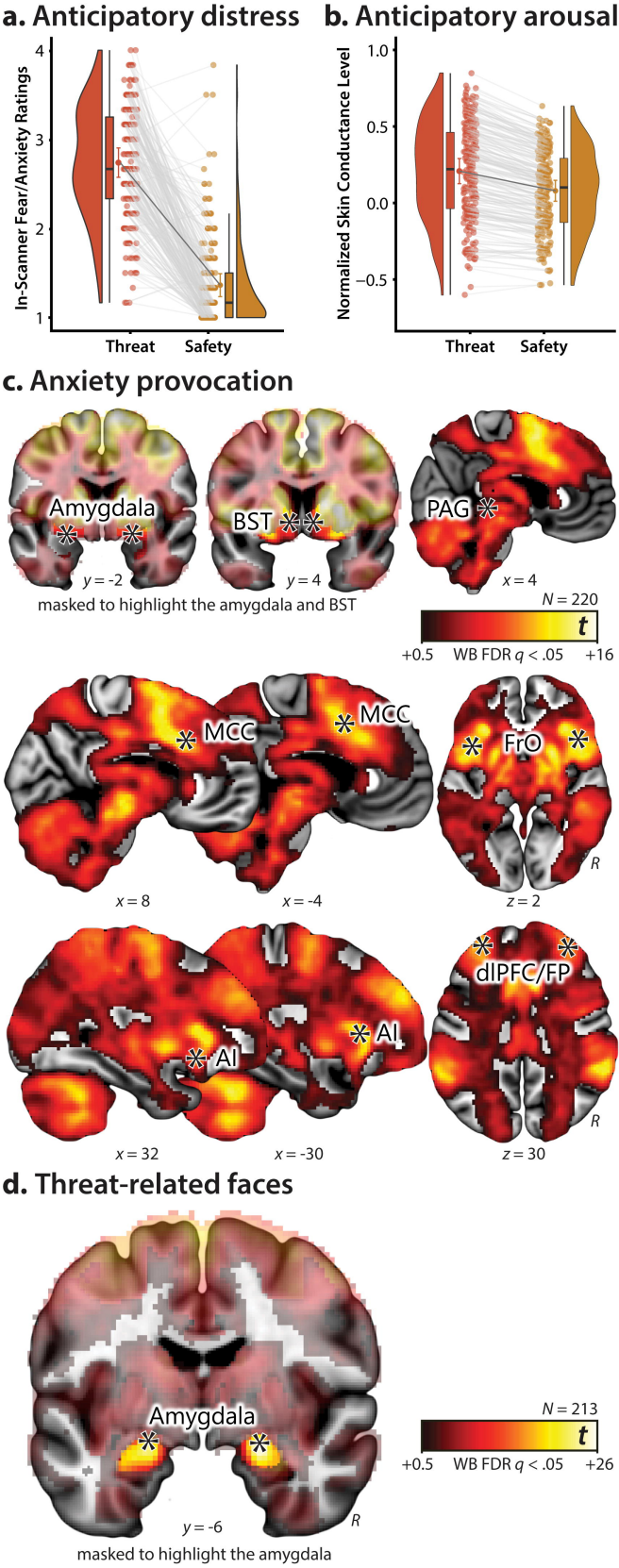
a. Anticipatory distress
In-Scanner Fear/Anxiety Ratings
4
3
2
1
Threat
Safety
b. Anticipatory arousal
Normalized Skin Conductance Level
1.0
0.5
0.0
−0.5
Threat
Safety
c. Anxiety provocation
Amygdala
y = -2
BST
y = 4
PAG
x = 4
masked to highlight the amygdala and BST
N = 220
t
+0.5
WB FDR q < .05
+16
MCC
MCC
x = 8
x = -4
FrO
R
z = 2
AI
AI
x = 32
x = -30
dlPFC/FP
R
z = 30
d. Threat-related faces
Amygdala
y = -6
R
masked to highlight the amygdala
N = 213
t
+0.5
WB FDR q < .05
+26

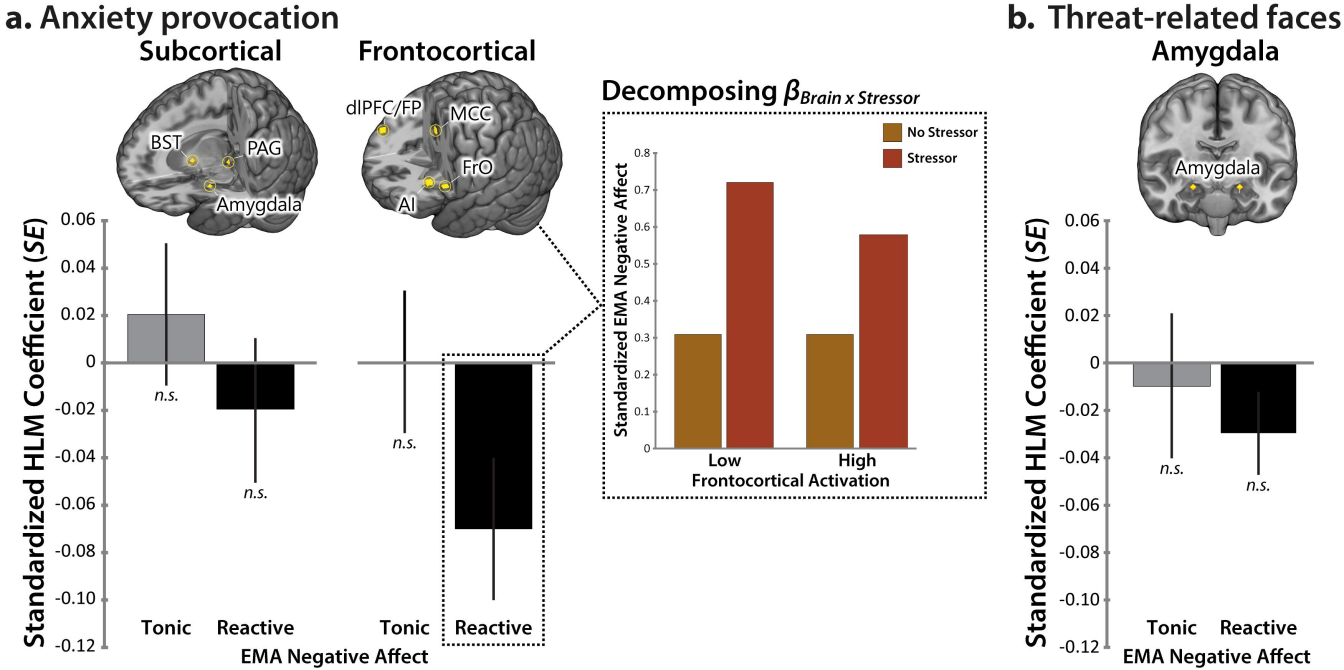
a. Anxiety provocation
Subcortical
Frontocortical
BST
PAG
Amygdala
dlPFC/FP
MCC
FrO
AI
Decomposing $\beta_{Brain\ x\ Stressor}$
No Stressor
Stressor
Standardized EMA Negative Affect
Low
High
Frontocortical Activation
Standardized HLM Coefficient (SE)
n.s.
n.s.
n.s.
n.s.
Tonic
Reactive
Tonic
Reactive
EMA Negative Affect
b. Threat-related faces
Amygdala
Amygdala
Standardized HLM Coefficient (SE)
n.s.
n.s.
Tonic
Reactive
EMA Negative Affect

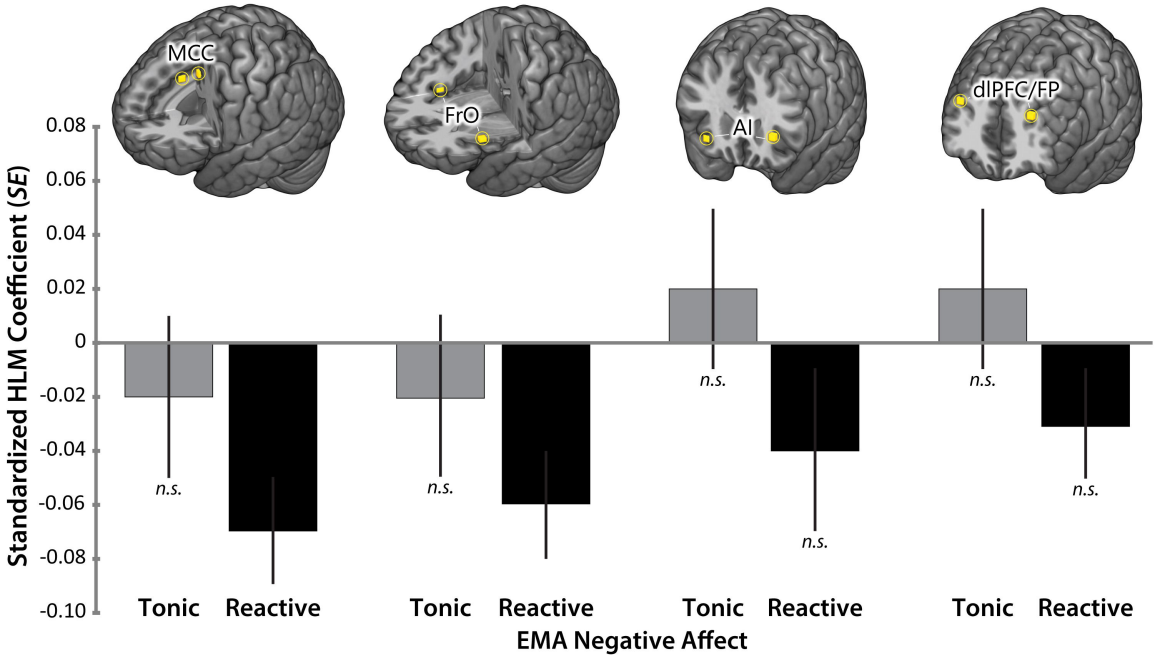
MCC
FrO
AI
dlPFC/FP
0.08
0.06
0.04
0.02
0
-0.02
-0.04
-0.06
-0.08
-0.10
Standardized HLM Coefficient (SE)
n.s.
n.s.
n.s.
n.s.
n.s.
n.s.
Tonic
Reactive
Tonic
Reactive
Tonic
Reactive
Tonic
Reactive
EMA Negative Affect

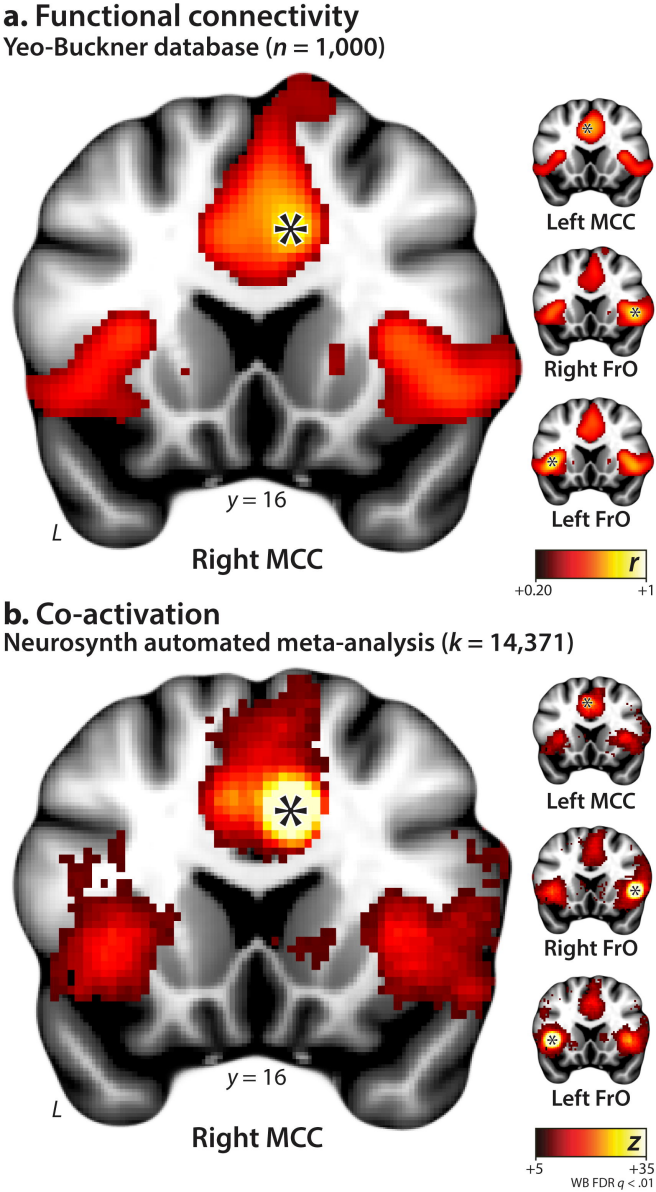
a. Functional connectivity
Yeo-Buckner database (n = 1,000)
Left MCC
Right FrO
Left FrO
y = 16
L
Right MCC
r
+0.20
+1
b. Co-activation
Neurosynth automated meta-analysis (k = 14,371)
Left MCC
Right FrO
Left FrO
y = 16
L
Right MCC
z
+5
+35
WB FDR q < .01